TUNGSTEN AND MOLYBDENUM OXIDATION KINETICS AT EXTREMELY HIGH TEMPERATURES

TECHNICAL DOCUMENTARY REPORT NO. ML-TDR-64-290
September 1964

Air Force Materials Laboratory
Research and Technology Division
United States Air Force
Wright-Patterson Air Force Base, Ohio

Project No. 7312, Task No. 731202

(Prepared under Contract No. AF 33(657)-8654
Philco Corporation, Research Laboratories
Newport Beach, California;
R. W. Bartlett, Author)

NOTICES

When Government drawings, specifications, or other data are used for any purpose other than in connection with a definitely related Government procurement operation, the United States Government thereby incurs no responsibility nor any obligation whatsoever; and the fact that the Government may have formulated, furnished, or in any way supplied the said drawings, specifications, or other data, is not to be regarded by implication or otherwise as in any manner licensing the holder or any other person or corporation, or conveying any rights or permission to manufacture, use, or sell any patented invention that may in any way be related thereto.

Qualified requesters may obtain copies of this report from the Defense Documentation Center (DDC), (formerly ASTIA), Cameron Station, Bldg. 5, 5010 Duke Street, Alexandria, Virginia, 22314.

This report has been released to the Office of Technical Services, U.S. Department of Commerce, Washington 25, D. C., for sale to the general public.

Copies of this report should not be returned to the Research and Technology Division, Wright-Patterson Air Force Base, Ohio, unless return is required by security considerations, contractual obligations, or notice on a specific document.

CLEARINGHOUSE FOR FEDERAL SCIENTIFIC AND TECHNICAL INFORMATION CFSTI
DOCUMENT MANAGEMENT BRANCH 410.11

LIMITATIONS IN REPRODUCTION QUALITY

ACCESSION # AD 609108

☒ 1. WE REGRET THAT LEGIBILITY OF THIS DOCUMENT IS IN PART UNSATISFACTORY. REPRODUCTION HAS BEEN MADE FROM BEST AVAILABLE COPY.

☐ 2. A PORTION OF THE ORIGINAL DOCUMENT CONTAINS FINE DETAIL WHICH MAY MAKE READING OF PHOTOCOPY DIFFICULT.

☐ 3. THE ORIGINAL DOCUMENT CONTAINS COLOR, BUT DISTRIBUTION COPIES ARE AVAILABLE IN BLACK-AND-WHITE REPRODUCTION ONLY.

☐ 4. THE INITIAL DISTRIBUTION COPIES CONTAIN COLOR WHICH WILL BE SHOWN IN BLACK-AND-WHITE WHEN IT IS NECESSARY TO REPRINT.

☐ 5. LIMITED SUPPLY ON HAND: WHEN EXHAUSTED, DOCUMENT WILL BE AVAILABLE IN MICROFICHE ONLY.

☐ 6. LIMITED SUPPLY ON HAND: WHEN EXHAUSTED DOCUMENT WILL NOT BE AVAILABLE.

☐ 7. DOCUMENT IS AVAILABLE IN MICROFICHE ONLY.

☐ 8. DOCUMENT AVAILABLE ON LOAN FROM CFSTI (TT DOCUMENTS ONLY).

☐ 9.

PROCESSOR:

TSL-107-10 64

FOREWORD

This is the final report prepared by Aeronutronic Applied Research Laboratory, Newport Beach, California, on Air Force Contract AF 33(657)-8654, Project No. 7312, Task No. 731202. This work was administered by the Air Force Materials Laboratory, Research and Technology Division. Mr. Paul Faust was project engineer. This report covers work from July 1, 1962 to July 1, 1964. The contractor's report number is U-2712.

Personnel participating in the work were Dr. R. W. Bartlett, Dr. W. M. Fassell, Dr. J. N. Ong, Jr., Mr. J. P. Pope, Mr. R. L. Johnson, Mr. R. S. Briggs, and Mr. R. W. Walker

ABSTRACT

An investigation to determine the processes, mechanisms and rates of oxidation of tungsten and molybdenum has been conducted with primary emphasis on tungsten. The study included four parts. (1) The oxidation rates of polycrystalline tungsten were measured at temperatures from 1300°C to near the melting point and oxygen pressures from 10^{-6} atm to 1 atm. The role of an inert gas diluent in depressing the oxidation rate was also determined. Results were correlated with (a) oxygen molecule sticking probabilities on hot tungsten and (b) oxygen diffusion (free convection) through the tungsten oxide vapor product boundary film adjacent to the tungsten surface. (2) The influence of forced convection from a hypersonic oxygen/argon stream on the oxidation rate was measured and correlated with forced convection theory. (3) Variation in the reaction probability with different tungsten crystal faces was determined using oriented single crystals. Differences in the surface morphology of tungsten faces after oxidation and the role of imperfections were observed. (4) The oxidation rates of polycrystalline molybdenum were measured at temperatures to near the melting point at the same oxygen pressures and using the same experimental methods employed in the initial tungsten study.

This technical documentary report has been reviewed and is approved.

I. Perlmutter

I. PERLMUTTER
Chief, Physical Metallurgy Branch
Air Force Materials Laboratory

TABLE OF CONTENTS

ILLUSTRATIONS

ILLUSTRATIONS (Continued)

NOMENCLATURE

d	=	Sample rod diameter
D_{AB}	=	Diffusivity of gases in boundary film (binary mixture)
E_a	=	Activation energy for temperature dependent oxidation rate
g	=	Acceleration of gravity
ΔH°	=	Standard reaction enthalpy
I	=	Moment of inertia oxygen molecule, equation (26)
J_{O_2}	=	Oxygen molecule wall collision flux
k	=	Boltzmann's constant
k_m	=	Coefficient for oxygen mass transfer through the boundary film
k', k''	=	Specific rate constants
K_1, K_2	=	Equilibrium constants
L	=	Characteristic length used in problem solving by dimensional analysis
m	=	Mass of molecule
M	=	Gram molecular weight
N	=	Surface density of tungsten atoms (Figure 15)
N_o	=	Avogadro's Number
R	=	Gas Constant
S	=	Sticking probability
T	=	Absolute temperature
v_∞	=	Free stream gas velocity
h	=	Plank's constant (equation 26)

X_W, X_{Mo} = Recession of metal surface

$\dot{X}_W$, $\dot{X}_{Mo}$ = Recession rate of metal surface

ϵ = Reaction probability

ρ = Density

$\bar{\rho}$ = Average gas density in the boundary film

σ = Oxygen molecule symmetry number, equation (26)

σ = Intermolecular force parameter used in Chapman-Enskog equations

Ω = Function for predicting transport properties using Chapman-Enskog equations

ζ = Pressure parameter in Grashof Number

μ_g = Gas viscosity

θ = Fraction of surface covered by chemisorbed oxygen

Subscripts

W = Tungsten

Mo = Molybdenum

∞ = Away from the metal surface and beyond the boundary film

(s) = At the surface

t = Total

O_2 = Oxygen molecule

WO_2 = WO_2 molecule

g = Average value for gas in boundary film

1 = First monolayer of chemisorbed oxygen

2 = Second monolayer of chemisorbed oxygen

Dimensionless Groups

Nu_{AB} = Nusselt Number for mass transfer; $Nu_{AB} = \dfrac{k_m L R T_g}{P_t D_{AB}}$

Gr_{AB} = Grashof Number for mass transfer;

$$Gr_{AB} = \frac{L^3 \bar{\rho}^2 g \zeta \Delta P_{O_2}}{\mu_g^2}$$

Re = Reynolds Number; $Re = \dfrac{L v_\infty \bar{\rho}}{\mu_g}$

Sc = Schmidt Number; $Sc = \dfrac{\mu_g}{\bar{\rho} D_{AB}}$

j_D = Chilton-Colburn dimensionless group for mass diffusion;

$$j_D = Nu_{AB} \, Re^{-1} \, Sc^{-1/3}$$

j_H = Chilton-Colburn dimensionless group for heat transfer;

$$j_H = Nu \, Re^{-1} \, Sc^{-1/3}$$

INTRODUCTION

Th hemistry of tungsten and molybdenum is similar, and experimental techniques itable for one of these metals are usually suitable for the other. Oxidation of both metals results in condensed oxide phases at moderate temperatures and gaseous oxide species at higher temperatures. Although several other condensed oxides of both tungsten and molybdenum are known, the oxides formed in situ are restricted to one suboxide, probably WO_2 and MoO_2, and the trioxides, WO_3 and MoO_3[1]. The observed gaseous species are monomers and polymers of the dioxides and trioxides[2-5]. These differences in oxidation products and additional variations in the chemical kinetic and transport processes associated with these oxidation products complicate the oxidation rate and have caused investigators to restrict their studies to temperature and pressure regimes where only one process is dominant.

Most of the previous tungsten oxidation rate studies have employed gravimetric methods and have been limited to temperatures below 1000°C where the weight loss associated with evaporation of tungsten oxides is negligible compared with the weight gain from oxidation[6-10]. The recent gravimetric studies of Gulbransen, Andrew, and Brassart[11] were extended to 1615°C by deducting weight loss due to oxide evaporation. Oxidation of tungsten below 1000°C is now fairly well understood[12]. Oxygen consumption rates have been determined at higher temperatures from pressure measurements, usually at constant flow rates, by Langmuir[13], Eisinger[14], Becker, Becker, and Brandes[15], and Anderson[16]. The sensitivity of this method decreases with increasing pressure; and, with the exception of Langmuir's work, these investigations were confined to pressures below 10^{-6} atm. Unfortunately, many desired Aerospace applications of tungsten are at either higher temperatures or higher pressures than studied by these investigators.

The history of molybdenum oxidation studies is similar to those for tungsten. Gravimetric techniques at low temperatures or pressure monitoring techniques at low pressures have been used exclusively[17-26].

Above approximately 1300°C, depending on the oxygen pressure, the rate of tungsten oxide evaporation is greater than the oxide formation rate; and recession of a tungsten surface can be measured optically without interference from an oxide layer. This technique was first used with molybdenum by Wilks[27] and with tungsten by Perkins and Crooks[28]. The latter investigators heated tungsten rods in air pressures from 1 to 40 Torr at temperatures between 1300°C and 3000°C. This method is more sensitive than the pressure monitoring method at pressures above 10^{-6} atm.

The present rate study emphasizes high temperatures, to near the melting points, and oxygen pressures from 10^{-6} to 1 atm. This range includes the temperature-pressure regime of interest for glide wing re-entry applications of tungsten. The optical surface recession technique was used. A diagram of the temperature-pressure regimes studied in this and previous studies is given, for tungsten in Figure 1 and for molybdenum in Figure 2. The authors for each study are indicated in the figures.

Manuscript released by author November, 1964 for publication as an R&D Technical Documentary Report.

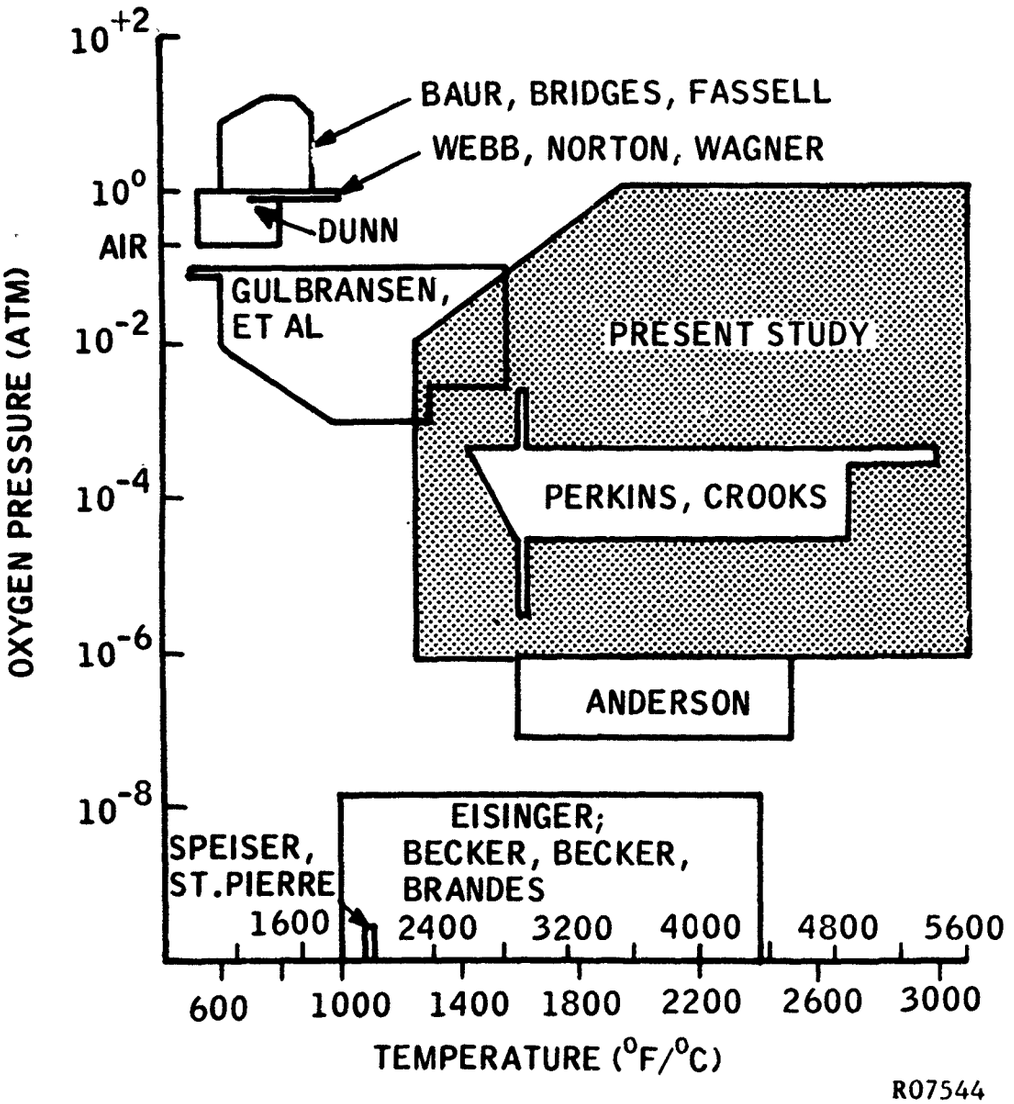

FIGURE 1. TEMPERATURE AND OXYGEN PRESSURE REGIMES EXPLORED BY THE PRINCIPAL INVESTIGATORS OF TUNGSTEN OXIDATION KINETICS

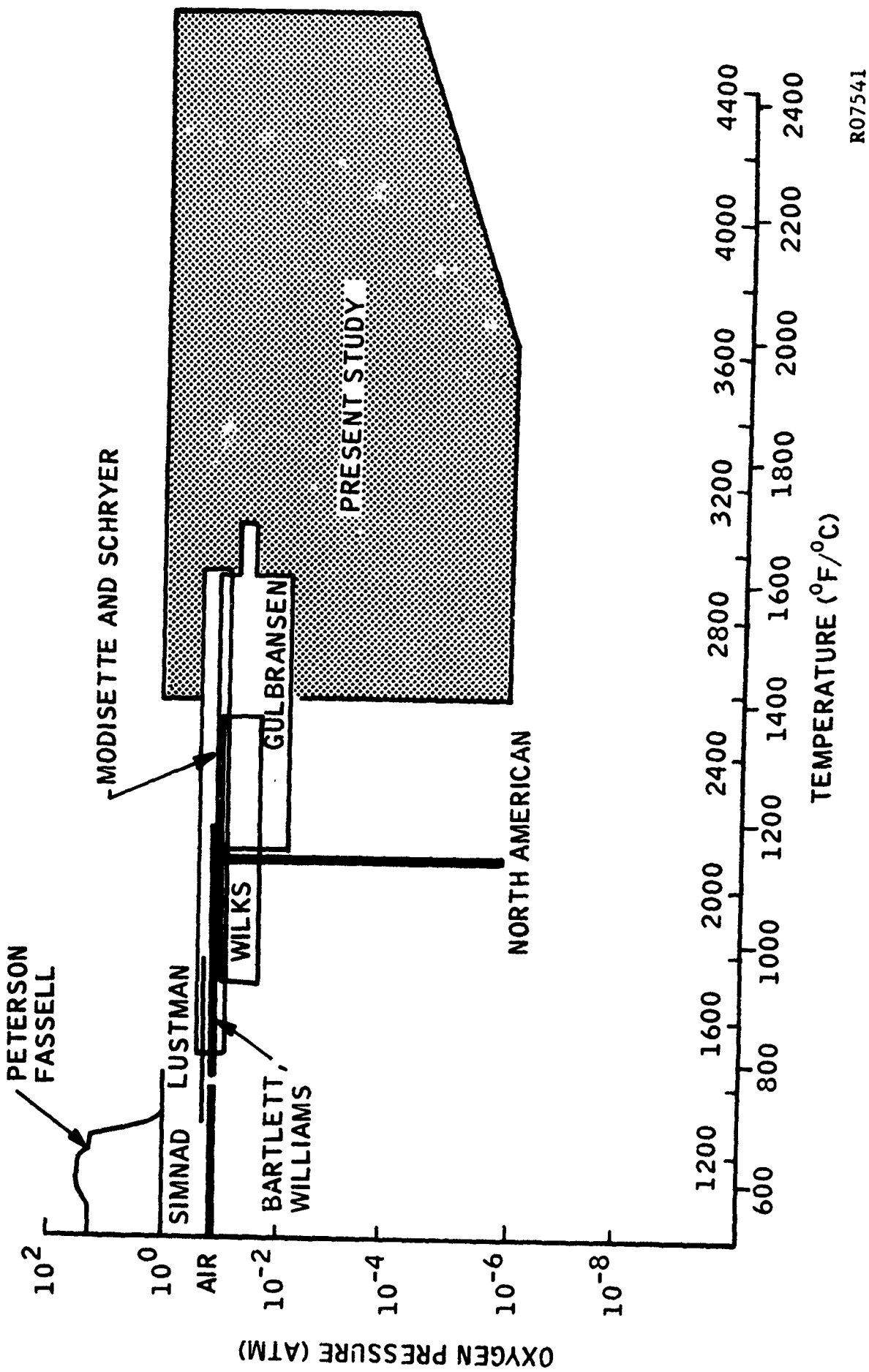

FIGURE 2. TEMPERATURE AND OXYGEN PRESSURE REGIMES EXPLORED BY THE PRINCIPAL INVESTIGATORS OF MOLYBDENUM OXIDATION KINETICS

Two other oxidation rate parameters, in addition to temperature and pressure, were studied extensively. These were (1) gaseous transport in the boundary layer adjacent to the oxidizing metal surface and (2) the crystal orientation of the metal. The results are divided into four sections. The first section reports the rates of oxidation of polycrystalline tungsten rods in a free convective gas environment as a function of temperature, oxygen pressure and pressure of an inert diluent gas. Rate mechanisms are proposed and satisfactorily correlated with the results. A second brief section reports tungsten oxidation rates in a forced convective environment using hypersonic gas flow over polycrystalline specimens. The third section covers the effect of crystal orientation on the rate of tungsten oxidation and the surface microstructure of tungsten as a result of oxidation. The fourth section reports rates of oxidation of polycrystalline molybdenum rods in a free convective oxygen environment. The kinetic studies of Sections 1 and 4 cover a wide variety of temperatures and pressures while the gas flow studies of Section 2 and the single crystal studies of Section 3 are more restricted, insofar as temperature and pressure variations are concerned.

SECTION 1

OXIDATION KINETICS OF POLYCRYSTALLINE TUNGSTEN

The purposes of the experiments described in this section were to determine the rate of recession of a tungsten surface in a variety of temperatures and oxygen pressures under conditions in which only gaseous oxide species were produced. The effect of an inert gaseous diluent, argon, in the boundary film was also studied. This particular gas was chosen because it has a molecular weight near nitrogen and can be used to simulate air in the boundary film adjacent to the sample without chemical side effects.

1. EXPERIMENTAL

Oxidation rates were determined by measuring the receding diameters of tungsten rods heated in the appropriate environment. Commercial ground seal rods with a length of 6 inches and an initial diameter of 0.125 inch were used as samples. These rods were heated by passing an electric current through them.

A. Apparatus

The apparatus used to conduct these experiments is a modification of the type used by Perkins and Crooks[28]. Rods were mounted vertically between two water cooled electrodes, one fixed and the other having free vertical travel. The movable counterweighted electrode was prevented from undergoing horizontal displacement by three sets of runners mounted at 120° intervals. Electrical contact was made by means of a water cooled mercury pool. The sample holder is shown in Figure 3. A 24-inch vacuum bell jar having a volume of approximately 267 liters was used as the reaction chamber surrounding the sample holder. Power was supplied from an 800 amp DC variable power supply.

Temperature readings were made by means of a two-color recording pyrometer*. With this instrument, corrections for emissivity are not necessary provided the spectral emissivities at two closely spaced wave lengths are equal. Supporting measurements were made with a micro-optical pyrometer corrected for the emissivity of bare tungsten and window absorptivity. The micro-optical pyrometer was calibrated against a National Bureau of Standards calibrated tungsten lamp and both pyrometers were periodically checked against the melting points of tungsten and molybdenum using the oxidation apparatus. Above 10^{-6} atm, pressures were measured with an Alphatron gauge calibrated against a McCleod gauge. At 10^{-6} atm, a Bayard-Alpert ionization gauge was employed.

---

*Latronics Model CMP3-26215

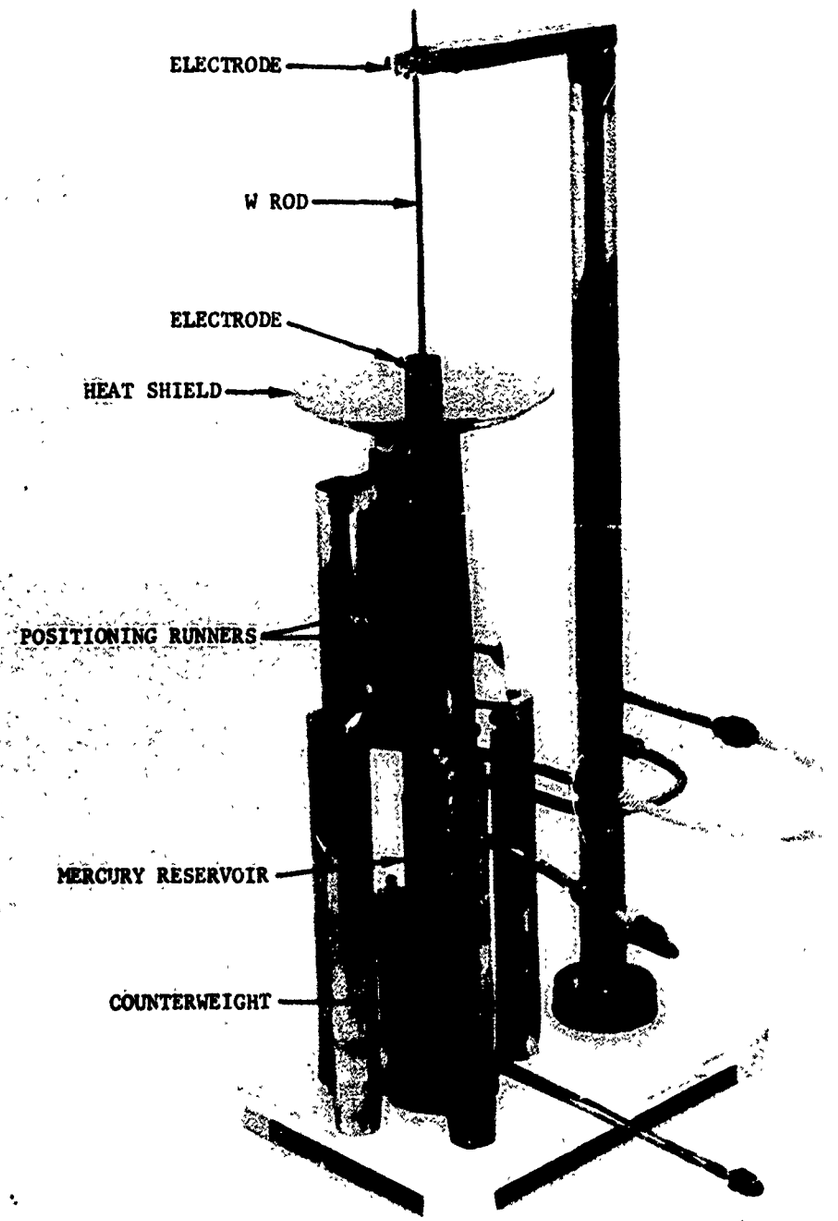

S12673

FIGURE 3. TUNGSTEN SAMPLE HOLDER SHOWING TWO WATER COOLED ELECTRODES, COUNTERWEIGHT AND SPRING LOADED POSITIONING RUNNERS

An image of the self illuminated tungsten rod was formed using a 360 mm objective lens mounted outside the bell jar. When the experiment exceeded one hour, this image was focused on a ground glass plate about ten feet from the tungsten rod at a magnification of about 8X and the recession of the thickness of this image was monitored with a Gaertner optical cathetometer. When faster rates were encountered, a time lapse 35 mm cine camera with a telephoto lens and bellows extension was substituted for the ground glass plate and cathetometer. Diameter recession rates were determined from the photographed image of the tungsten rod projected on the screen of an analytical film reader. A schematic of the experimental apparatus is shown in Figure 4.

B. Procedure

After installing the rod in the apparatus and cleaning it with acetone, the system was evacuated to $< 1 \times 10^{-5}$ Torr. Before oxygen was introduced, power was supplied to the filament to permit outgassing of the specimen and focusing of the pyrometer and optical train. These were located opposite each other on a common horizon which bisected the tungsten rod. When oxygen pressures as high as 10^{-2} atm were required, the amount of oxygen consumed during a run was less than 5 per cent of the chamber reservoir and gases could be precharged. At pressures below 10^{-2} atm, a continuous flow of oxygen was required with inlet and outlet rates manually controlled during the experiment to maintain the desired pressure. Continuous pumping wasted most of the oxygen but prevented gas impurities or water vapor, desorbed from the chamber walls, from accumulating in the reaction chamber. When argon was required, it was either added to the reaction chamber after the oxygen or premixed with oxygen in a separate pressure vessel prior to flowing through the reaction chamber. Flow rates were adjusted to prevent a decrease of more than five per cent in the oxygen mole fraction in the gas stream due to sample gettering. Water vapor and condensible impurities were also removed from both gases prior to entering the chamber by a cold trap immersed in a dry ice and acetone mixture.

Power was rapidly applied at the start of each experiment. However, because of the initial low electrical resistance of tungsten, about 10 seconds elapsed before the rod became incandescent. Approximately 15 per cent of the rod was removed in each experiment with the runs lasting from 30 seconds to 15 hours. At the completion of each run conducted at higher pressures, the rod was quenched with argon to prevent continued burning. Final diameters were measured with an optical comparitor or precision micrometer and checked against the same results accumulated optically during the experiments.

2. MATERIALS

Systematic rate differences between unetched ground seal rods supplied by General Electric Company and etched ground seal rods supplied by Sylvania Electric Products, Inc., were not observed. Spectrographic analyses of the tungsten lots used are given in Table 1. The 0.040 inch diameter rods were used in lieu of the 0.125 inch rods for a few extended high temperature experiments to prevent overheating the bell jar. All of the materials had

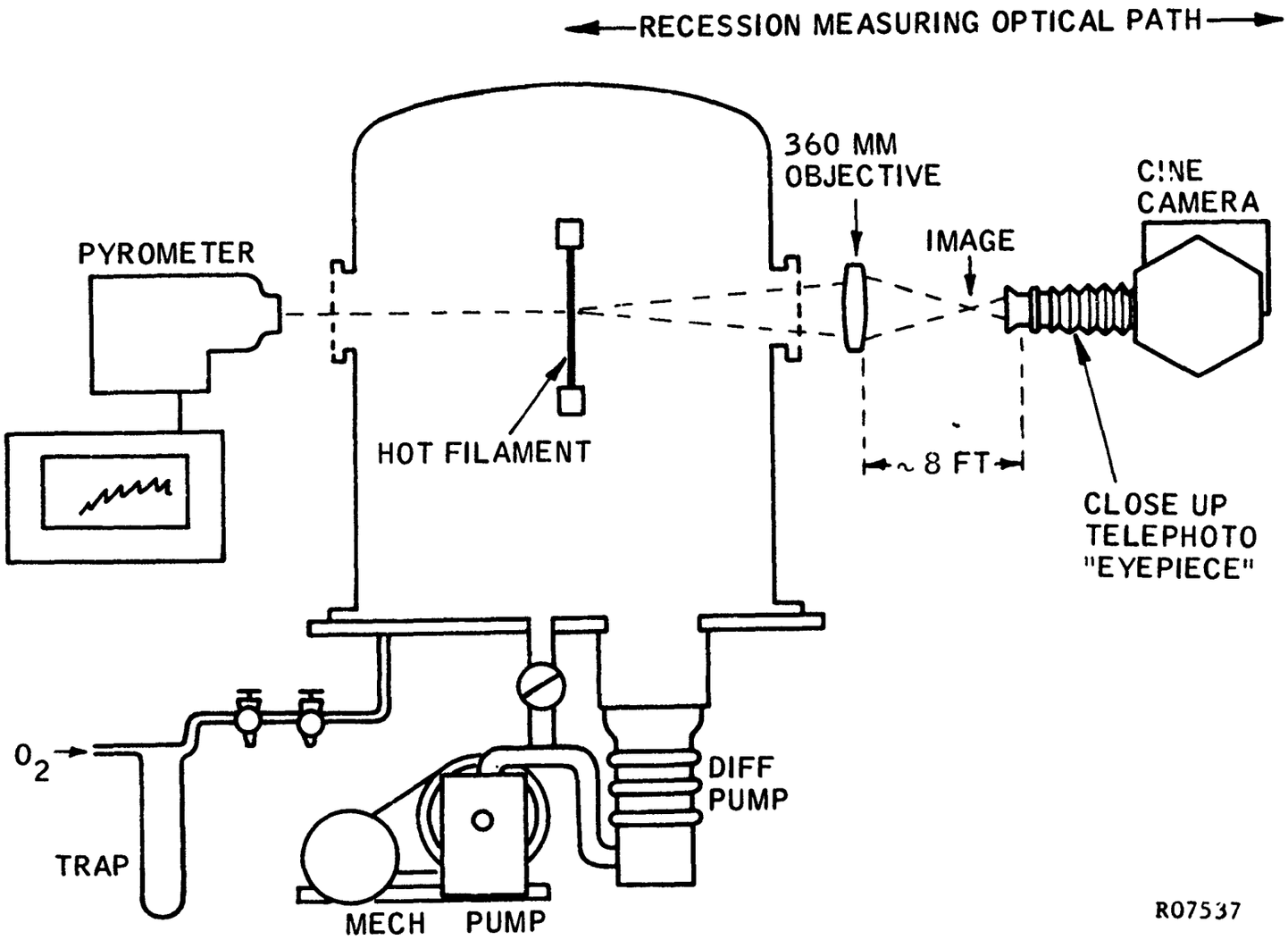

FIGURE 4. APPARATUS FOR DETERMINING OXIDATION RATES OF TUNGSTEN FILAMENTS

TABLE 1

SPECTROGRAPHIC ANALYSIS OF TUNGSTEN GROUND SEAL RODS

	General Electric 0.125"	Sylvania 0.125"	Sylvania 0.040"
Tungsten	Remainder	Remainder	Remainder
Silicon	0.036%	0.003%	0.034%
Boron	0.32	nil	nil
Magnesium	0.019	nil	0.0048
Iron	0.007	0.006	0.006
Aluminum	0.32	nil	nil
Beryllium	0.0012	nil	nil
Copper	0.0012	nil	nil
Calcium	0.012	nil	0.0024
Other Elements	nil	nil	nil

elongated grains typical of a swaged or drawn metal rod and occasional microcracks were present parallel to the axis of the rods.

3. RESULTS

Rate measurements were made at eight approximately equal increments of reciprocal temperature between 1320°C and 3170°C, and at oxygen-pressure decades between 1 x 10^{-6} atm and 1 atm, inclusive. Various mixtures of oxygen and argon were employed. In all cases, the rate was linear as illustrated by the typical experimental data of Figure 5 in which tungsten filament recession is plotted against the elapsed time of the experiment. An Arrhenius plot of the rate data versus reciprocal absolute temperature is shown in Figure 6. These data are for experiments conducted in pure oxygen at the pressures indicated. The apparent rate increases appearing in the lower left hand corner of Figure 6 were caused by evaporation of tungsten. The rates of evaporation measured in this laboratory at less than 1 x 10^{-7} atm total pressure are also shown in Figure 6. Otherwise, these data represent the actual oxidation rates under the specified temperature and pressure conditions.

Recrystallization of the tungsten occurred after prolonged heating at high temperatures. Tests performed in a hard vacuum indicated that recrystallization did not directly affect the sample diameters. However, the oxidation rates do vary with crystal orientation and recrystallization was expected to influence the oxidation rate somewhat. The expected effect, either an increase or decrease in rate (non-linearity) as recrystallization occurred, was not observed. Rather, the oxidation rates for polycrystalline tungsten were close to the lowest oxidation rates observed on tungsten faces. The elongated grain structure of the tungsten rods before heating is shown in both the transverse and longitudinal directions in Figure 7 along with the same views of a tungsten rod after oxidation for seven hours at 2750°C. The grain size after oxidation was uniform across the rod.

At 10^{-3} atm, the tungsten rods have a colored metallic luster which varies from gold through several hues of purple and blue. Back reflection pin hole X-ray investigation indicates the presence of only tungsten, although the characteristic Debye rings are less sharp than usual. Evidently, an amorphous oxide film whose thickness is of the order of the wave length of the reflected light is formed. At higher pressures, the surface is a dull dark gray, while at lower pressures the surface is clean. Because the oxide films formed above 10^{-3} atm did not exhibit any characteristics dependent on the temperature and duration of the experiment, they are believed to have formed during cooling.

X-ray diffraction analyses of forty-three samples of the oxide powder collected in the vacuum chamber after experiments indicate that WO_3 is the principal phase present. Unidentified peaks at 3.69A and 1.847A suggest the presence of the 770°C form of WO_3 and possibly some $W_{18}O_{49}$. Distinct diffraction peaks were observed at 10^{-2} atm, but line broadening becomes very appreciable at 10^{-3} atm. At 10^{-4} atm, the oxide appears amorphous.

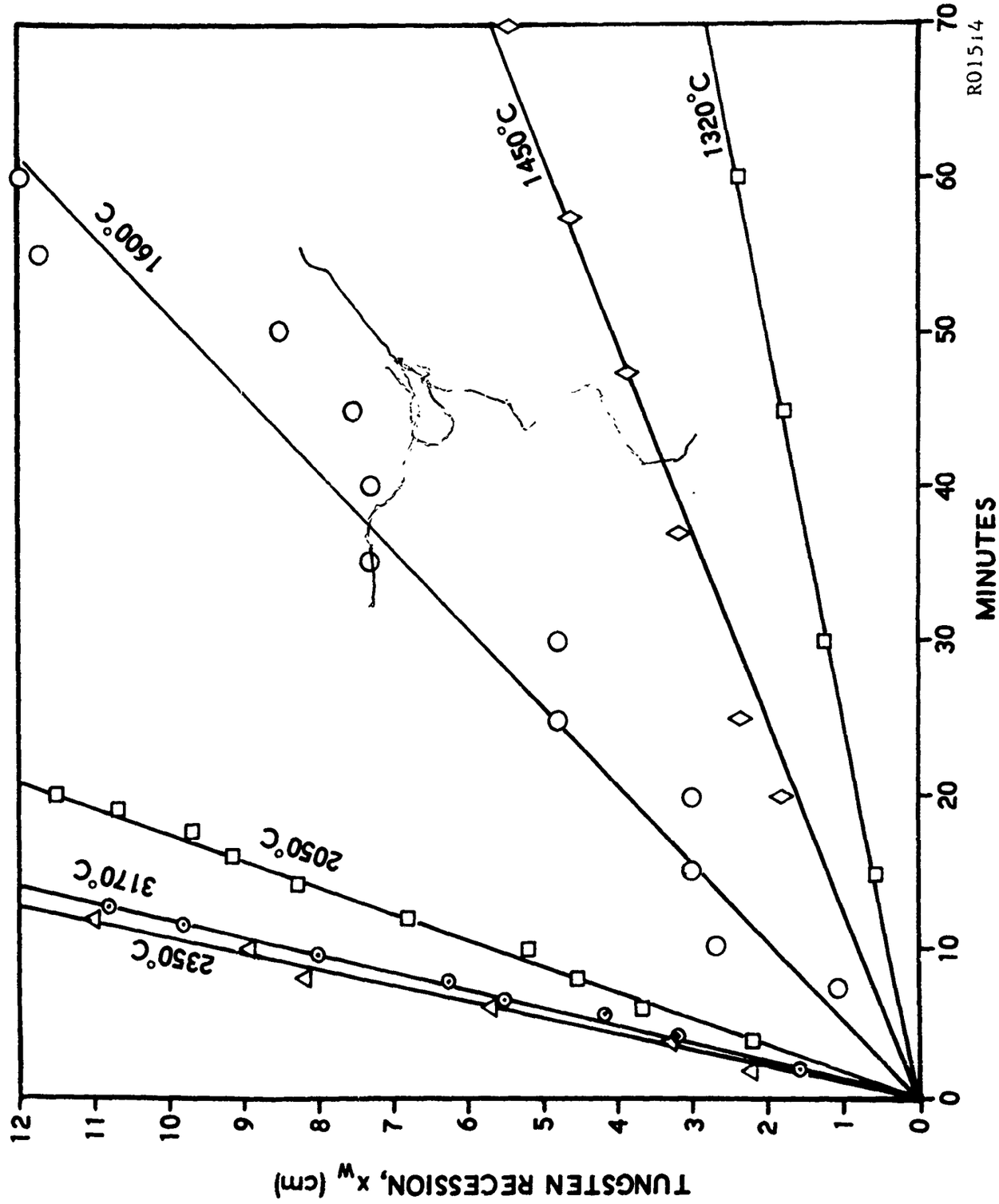

FIGURE 5. RADIUS RECESSION OF TUNGSTEN ROD AT $P_{O_2} = 1 \times 10^{-4}$ ATM

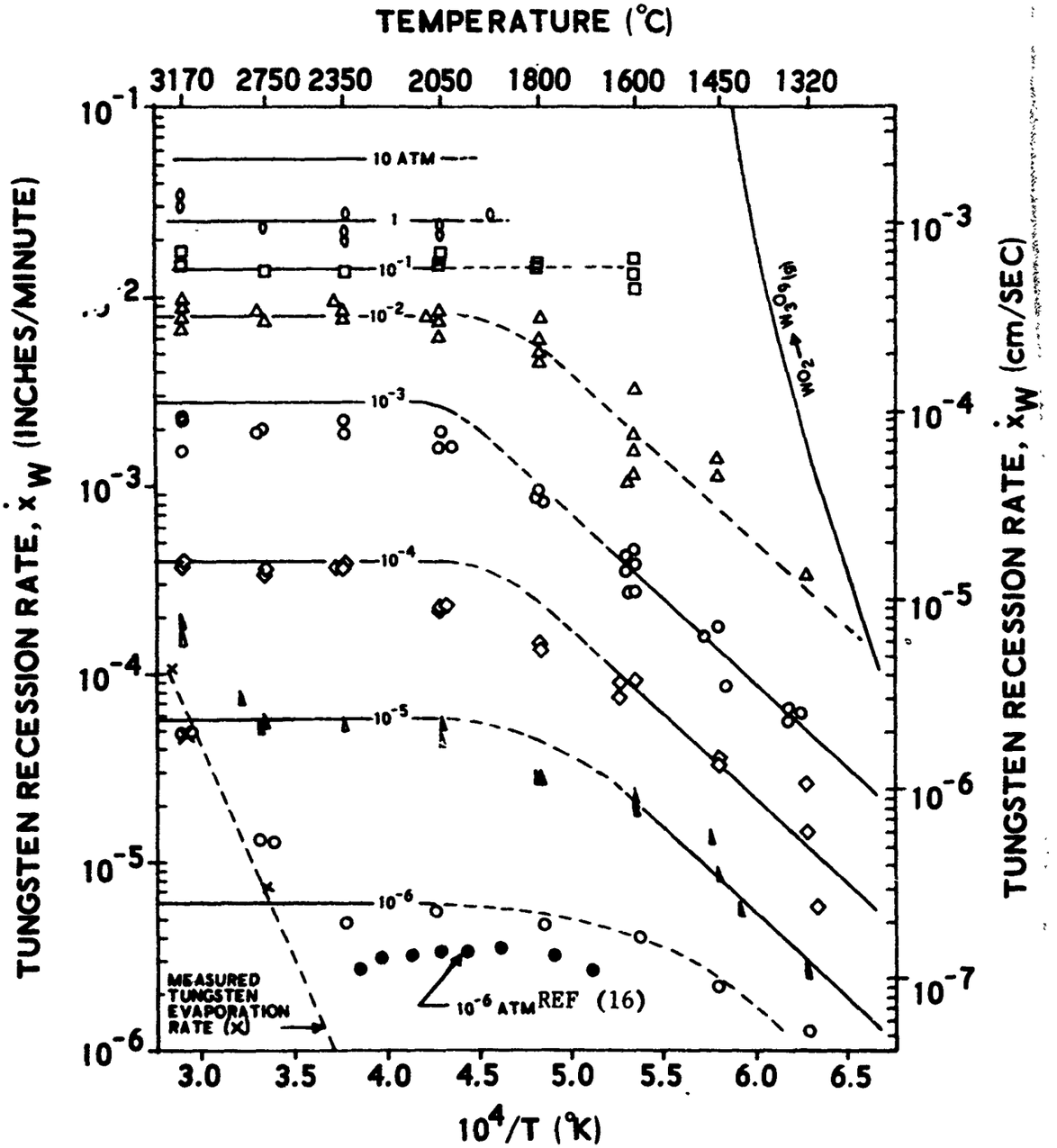

FIGURE 6. ARRHENIUS PLOT OF TUNGSTEN RECESSION RATE VERSUS RECIPROCAL ABSOLUTE TEMPERATURE IN OXYGEN: HORIZONTAL LINES OF LEFT HAND SIDE ARE BASED ON THEORETICAL PREDICTIONS, SEE FIGURE 10

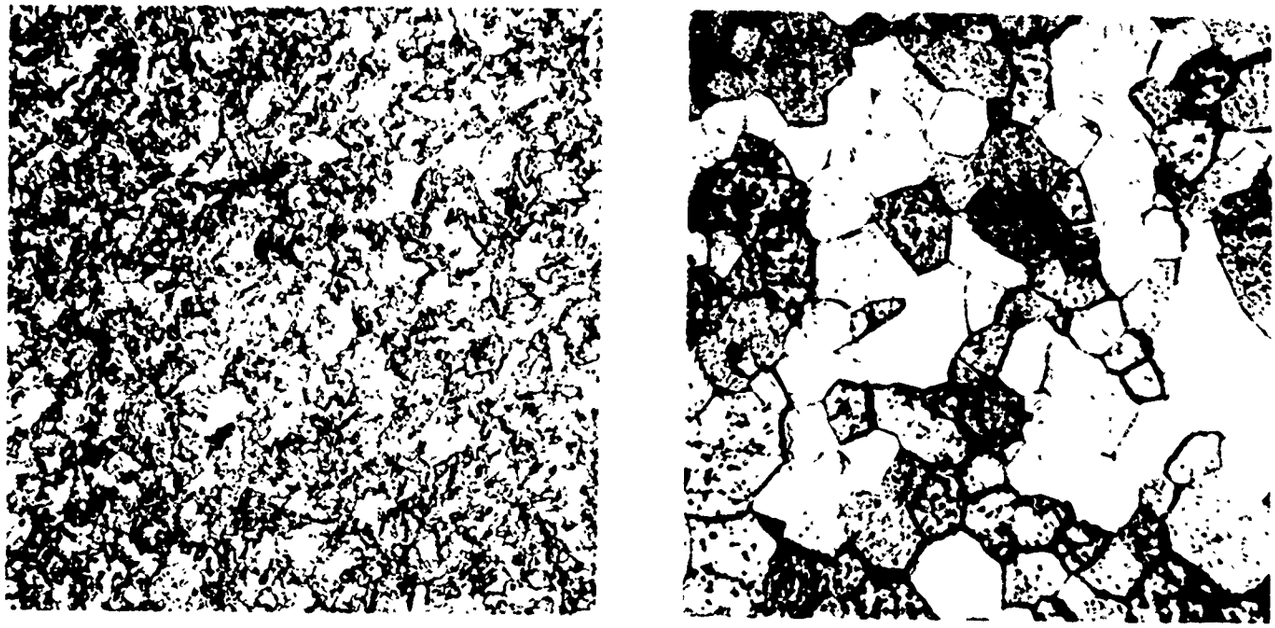

FIGURE 7. TRANSVERSE AND LONGITUDINAL VIEW OF TUNGSTEN GRAIN STRUCTURE BEFORE AND AFTER OXIDATION 7 HOURS AT 3170°C

4. ANALYSIS OF RATES ABOVE 2000°C, BOUNDARY FILM EFFECTS

Above about 2000°C, the oxidation rate is independent of temperature. This is in good agreement with the data of Langmuir[13] and in reasonable agreement with the later work of Perkins, Price and Crooks[29] in which only a small rate decrease with increasing temperature was observed. The oxidation rate dependence on oxygen pressure is complex. Below 10^{-5} atm, the rate is directly proportional to the oxygen pressure. At higher oxygen pressures, the rate increments caused by each pressure increment are less pronounced. These temperature and pressure relations suggest that the oxidation rate above 2000°C is affected by oxygen transport through a boundary film to the surface.

In the molecular flow pressure range, below 10^{-5} atm, the oxidation rate can be calculated from the number of oxygen molecule collisions with the sample using gas kinetic theory. This calculation requires knowledge about the average stoichiometry of the oxide vapor products. Recently, Berkowitz-Mattuck, et al.,[30] have made a mass spectrometric study of the oxide vapor species evolved from hot tungsten surfaces. Their technique provided for sampling the vapor species before subsequent collisions and reactions in the gas phase altered the gas composition. They found that $WO_2(g)$ was the most prevalent product above 2000°C with some $WO_3(g)$ also being produced. Tungsten oxide polymers are evidently produced only by secondary collisions in the gas phase. If this chemistry is assumed for the primary reaction,

$$W + O_2 \rightleftarrows WO_2(g) \tag{1}$$

one tungsten atom is removed for each reacting oxygen molecule. The tungsten surface recession rate can be calculated from the oxygen collision flux, J_{O_2}, which is given by gas kinetic theory (Hertz-Knudsen equation):

$$J_{O_2} = P_{O_2} / (2\pi mkT)^{\frac{1}{2}} \tag{2}$$

where P_{O_2} is the oxygen pressure, m is the mass of an O_2 molecule, k is Boltzmann's constant and T is absolute temperature. The tungsten recession rate is related to the oxygen flux, the gram molecular weight of tungsten, M_W, the density of tungsten, ρ_W, and a reaction probability that an oxygen molecule experiencing collision with the tungsten surface will react with tungsten, $\epsilon \leq 1$. The tungsten recession rate, $\dot{X}_W$, is:

$$\dot{X}_W = \frac{\epsilon}{\rho_W} \left(\frac{M_W}{N_o} \right) J_{O_2} \tag{3}$$

If the oxygen pressure is conveniently expressed in atmospheres, a conversion factor, 1.01×10^6 dynes cm^{-2}/atm, must be inserted in the right side of equation (2) and the net result is the following equation

$$\dot{X}_W = \epsilon \nu_0 P_{O_2} \quad \text{(cm/sec)} \tag{4}$$

where ν_0 consolidates the constants of equations (2) and (3); $\nu_0 = 75(T^{-\frac{1}{2}})$.

Equation (4) gives a direct pressure dependence which is not observed above $P_{O_2} = 10^{-5}$ atm. At higher oxygen pressures a surface boundary film will be formed by the rapid evolution of tungsten oxide vapors. The effect of this boundary film is to perturb the oxidation rate by depressing the oxygen pressure at the tungsten surface, $P_{O_2}(s)$ to a lower pressure than the oxygen pressure beyond the boundary film, $P_{O_2 \infty}$. The latter oxygen pressure is simply the system pressure within the reaction chamber and can be measured directly. However, the oxygen pressure experienced by the surface is the pertinent oxygen pressure to equation (4) and this cannot be measured directly.

Since oxygen transport through the boundary film is a necessary step prior to oxidation, the surface oxidation rate and the net oxygen transport rate through the boundary film must be equal. Oxygen transport through the boundary film is related to a mass transfer coefficient, k_m, the difference in oxygen pressure across the boundary film and the total pressure, P_t. In terms of the equivalent tungsten recession, this provides the following rate:

$$\dot{X}_W = \frac{k_m \left[P_{O_2 \infty} - P_{O_2(s)} \right]}{P_t} \frac{M_W}{\rho_W} \tag{5}$$

A schematic of the relationship of the boundary film to the oxidation rate process is shown in Figure 8. The mass transfer coefficient, k_m, is analogous to more familiar heat transfer coefficients. These transfer coefficients cannot be rigorously derived but can be obtained for boundary films about simple geometries using correlations obtained by combining experimental results with the results of dimensional analysis.

As a consequence of this approach, the mass transfer coefficient, k_m, is normally related to the Nusselt number, Nu_{AB}, by the following defining relation for a binary mass transfer system,

$$Nu_{AB} = \frac{k_m L R T_g}{P_t D_{AB}} \tag{6}$$

where L is a characteristic dimension, R is the gas constant, D_{AB} is the diffusivity and T_g is the average gas temperature of the boundary film. Inserting the temperature and pressure dependence of the diffusivity,

$$D_{AB} = \frac{D_{AB_o} T_g^{3/2}}{P_t} \tag{7}$$

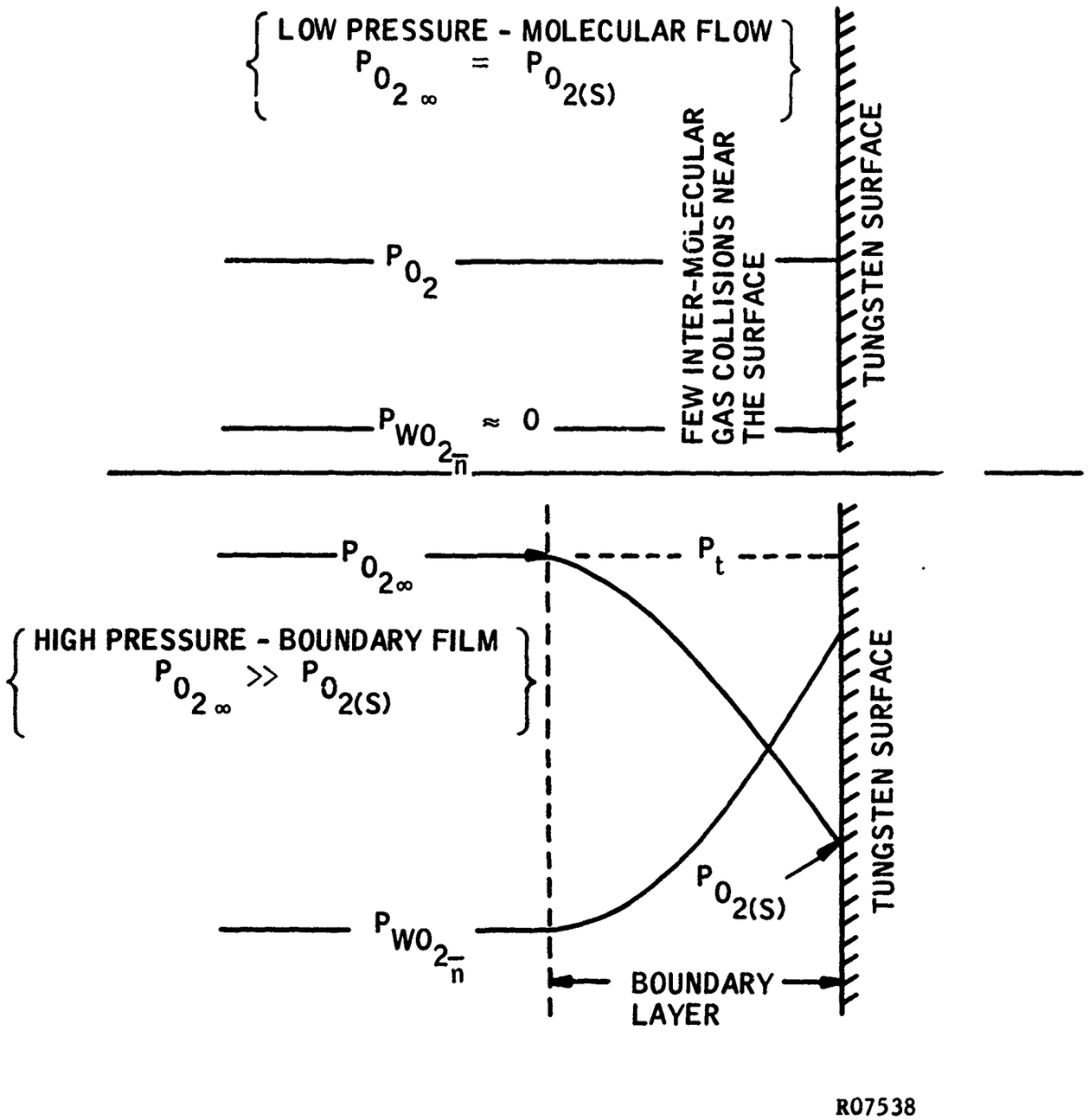

FIGURE 8. OXYGEN TRANSPORT TO THE SURFACE IN THE MOLECULAR FLOW RANGE (LOW PRESSURES) AND THROUGH A BOUNDARY FILM (HIGH PRESSURES) FORMED BY THE OXIDE VAPOR SPECIES PRODUCED. BOTH CASES ARE FOR OXIDATION IN PURE OXYGEN.

provides the following rate equation:

$$\dot{X}_W = \frac{M_W \, Nu_{AB} \, D_{AB_o} \, T_g^{\frac{1}{2}}}{\rho_W \, L \, R} \left\{ \frac{P_{O_{2\infty}} - P_{O_{2(s)}}}{P_t} \right\} \qquad (8)$$

Thus, we have two equations for the oxidation rate, equations (4) and (8), and a rate equation can be formed which eliminates the unknown surface pressure term. When equation (4) is used to substitute for $P_{O_{2(s)}}$ in equation (8) the following rate equation results:

$$\dot{X}_W = \frac{\epsilon \nu_o \, P_{O_{2\infty}}}{1 + \frac{\epsilon \nu_o \, P_t}{C_o \, Nu_{AB}}} \qquad (9)$$

where C_o is a combined constant; $C_o = \frac{M_W \, D_{AB_o} \, T_g^{\frac{1}{2}}}{\rho_W \, L \, R}$.

The constants in equation (9) must be evaluated so that a theoretical plot of $\dot{X}_W$ versus $P_{O_{2\infty}}$ can be constructed and compared with the experimental results.

The Nusselt number, ordinate, is plotted versus the product of the Grashof and Schmidt numbers, abscissa, in Figure 9. This curve is a semi-empirical free convection correlation for either flat vertical surfaces or horizontal cylinders, L = d, that has been verified for several fluids[31]. The following Chapman-Enskog equations[32] were used to calculate the diffusivity and viscosity in the boundary film:

$$D_{AB} = \frac{1.86 \times 10^{-3} \left(\frac{1}{M_{O_2}} + \frac{1}{M_{WO_2}} \right)^{\frac{1}{2}}}{\sigma_{AB}^2 \, \Omega_D} \left(\frac{T_g}{P_t} \right)^{3/2} \qquad (10)$$

$$\mu_g = 2.67 \times 10^{-5} \frac{\sqrt{M_{O_2} \, T_g}}{\sigma^2 \, \Omega_\mu} \qquad (11)$$

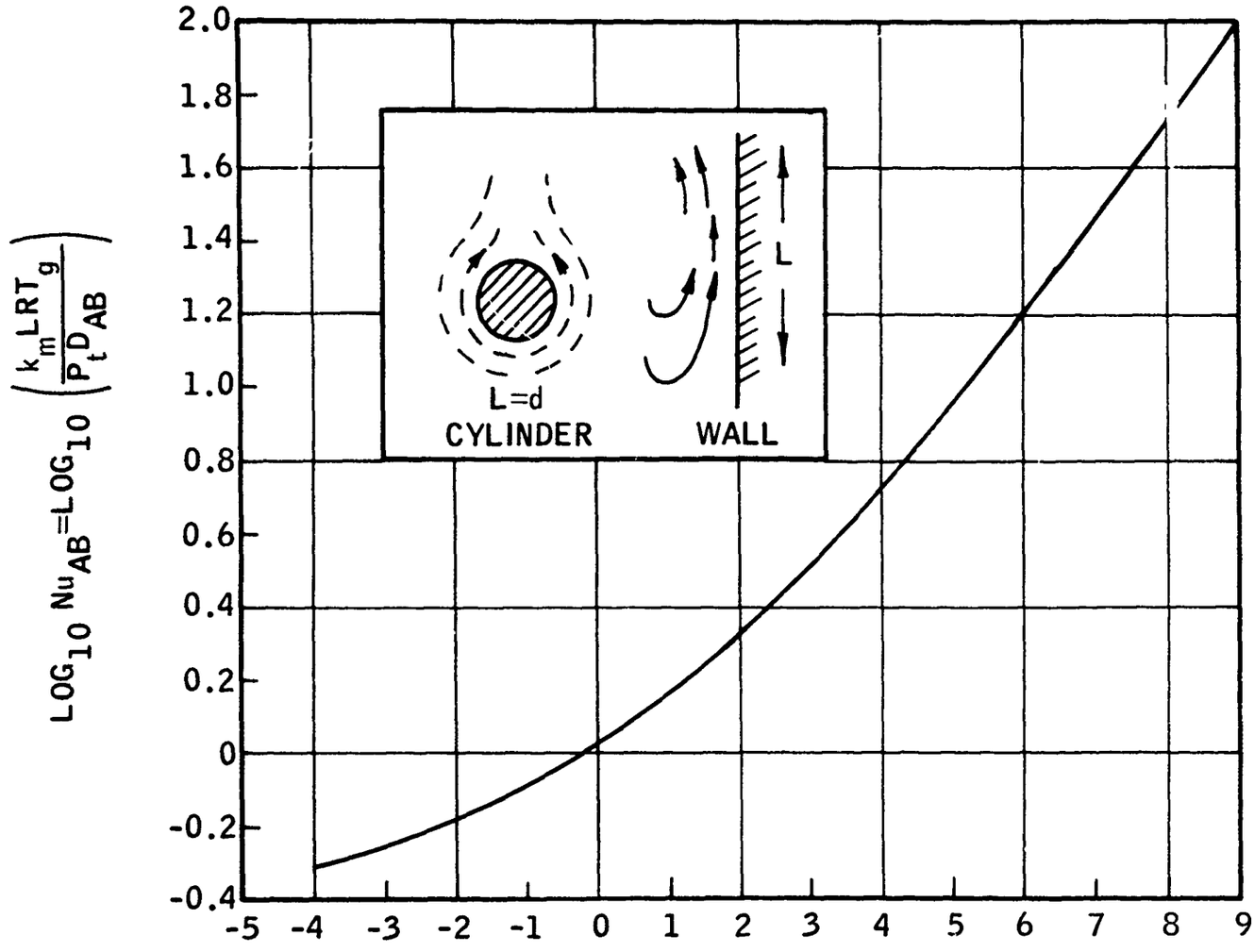

$$LOG_{10}\left(Gr_{AB} Sc\right) = LOG_{10}\left\{\left(\frac{L^3 \bar{\rho}^2 g \zeta \Delta P_{O_2}}{\mu_g^2}\right)\left(\frac{\mu_g}{\bar{\rho} D_{AB}}\right)\right\}$$

R07542

FIGURE 9. FREE CONVECTION CORRELATION FOR VERTICAL SURFACES AND HORIZONTAL CYLINDERS, CHARACTERISTIC LENGTH L EQUALS DIAMETER "d"

Because of lack of data for tungsten oxides the values for O_2 were assumed for the Chapman-Enskog intermolecular force parameter, σ, and transport prediction function, Ω. Since variations in these parameters between gases are slight, errors introduced by this approximation should be negligible. The value of ζ for ideal gases was assumed,

$$1/\zeta = \left\{ \frac{P_{O_2\infty} + P_{O_2(s)}}{2} \right\} .$$

The boundary film temperature T_g was assumed to be $\frac{T_\infty + T_s}{2}$. Unfortunately, a Nusselt number correlation curve for thin vertical cylinders is not available. As the height of the incandescent zone varied somewhat and was not of uniform temperature, two values of the characteristic length were assumed for computing theoretical rates: the rod diameter, 0.32 cm, and the approximate height of the hot zone, 3 cm. An extensive treatment of transport in boundary films is given in reference 32, Chapters 13 and 21. A table of values for the intermolecular force constants and transport prediction functions is included.

The reaction probability constant, ϵ, was determined from the data at 10^{-6} atm using equation (4) and has a value of 0.06. No other constants based on the experimental data are employed in the theory, equation (9), which is plotted for pure oxygen, $P_{O_2\infty} = P_t$, and compared with the experimental data in Figure 10. Several mixtures of oxygen and argon using the appropriate Chapman-Enskog constants for argon are also compared with the equivalent experimental data in Figure 10. The agreement between the experimental data and the theoretical curves, with and without the argon diluent, supports the validity of equation (9) and the free convection boundary layer and constant reaction probability premises upon which it is derived.

5. ANALYSIS OF OXIDATION RATES BELOW 2000°C - TEMPERATURE DEPENDENCE

Below about 1800°C, the oxidation rate decreases with decreasing pressure. However, it was difficult to obtain data at high pressures and low temperatures because of the nucleation and growth of WO_3 nodules on the surface of the tungsten rods. Hertz-Knudsen effusion rate calculations based on the equilibrium vapor pressure[33] of the most predominant vapor species in equilibrium under these conditions, $W_3O_9(g)$, indicate that condensed oxides should not be present. The sublimation rate curve for the most stable solid oxide, WO_2, is shown in the upper right corner of Figure 6. However, the calculated rates assume that none of the oxide molecules will be reflected back to the sample and condense. This is unlikely at the high oxygen pressures involved and the true rates of sublimation are probably lower. It was also evident that the WO_3 nodules were much cooler than the tungsten rod. They tended to extend into the gas phase with very little contact at the tungsten surface. An example of this effect is shown in Figure 11 which is a photograph of an oxidized tungsten rod taken after cooling. Increased temperature decreases the number of nodules but increases their average size. This temperature dependence conforms with the accepted theory for homogeneous nucleation and growth in which increased temperature increases the growth rate of critically sized nuclei while at the same time decreasing the number which reach critical size[34].

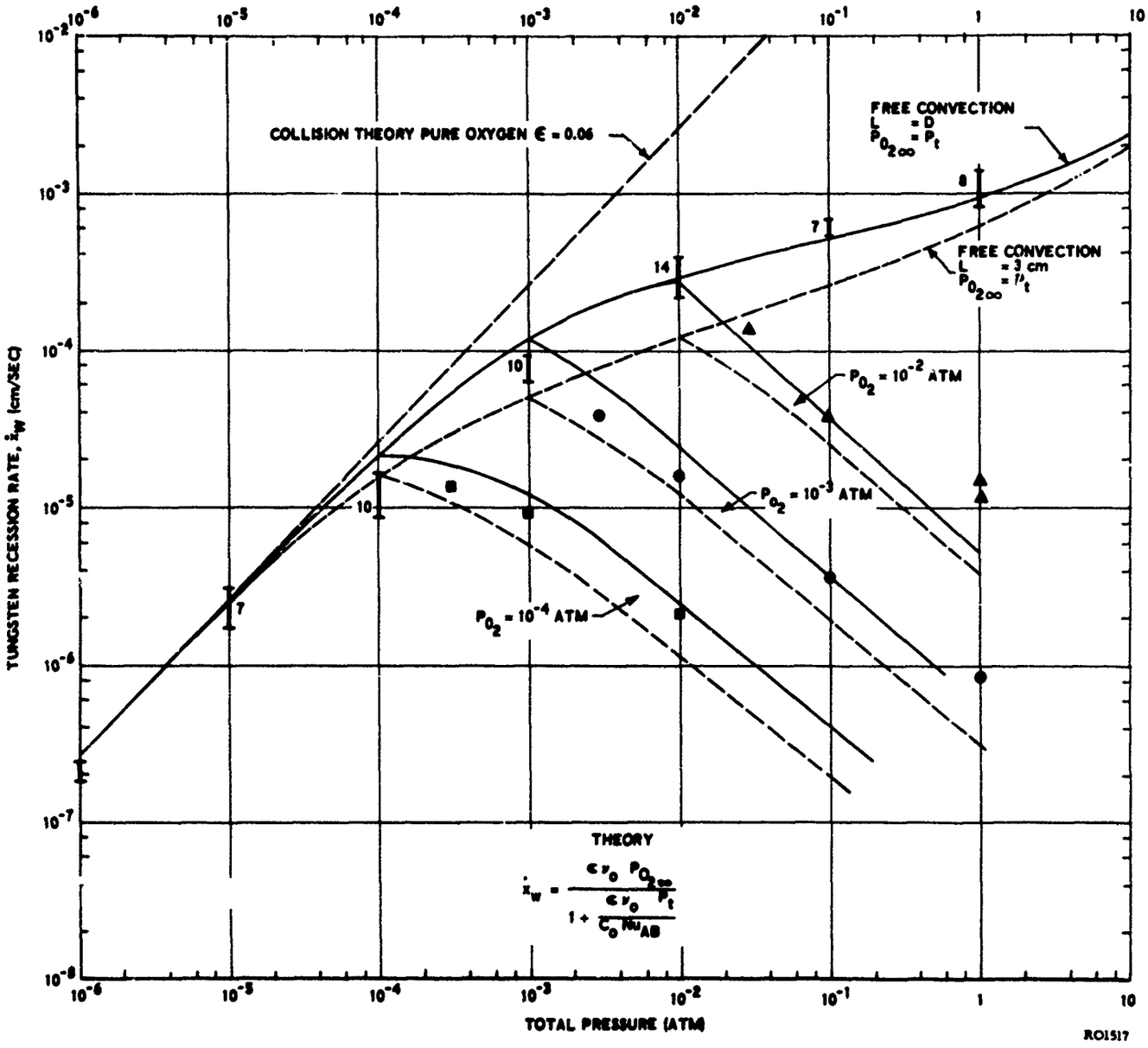

FIGURE 10. EXPERIMENTAL AND THEORETICAL PRESSURE DEPENDENCE OF THE TUNGSTEN OXIDATION RATE ABOVE 2000°C

R01518

FIGURE 11. WO_3 NODULES GROWING ON TUNGSTEN AT 1320°C AND $P_{O_2} = 10^{-3}$ ATM

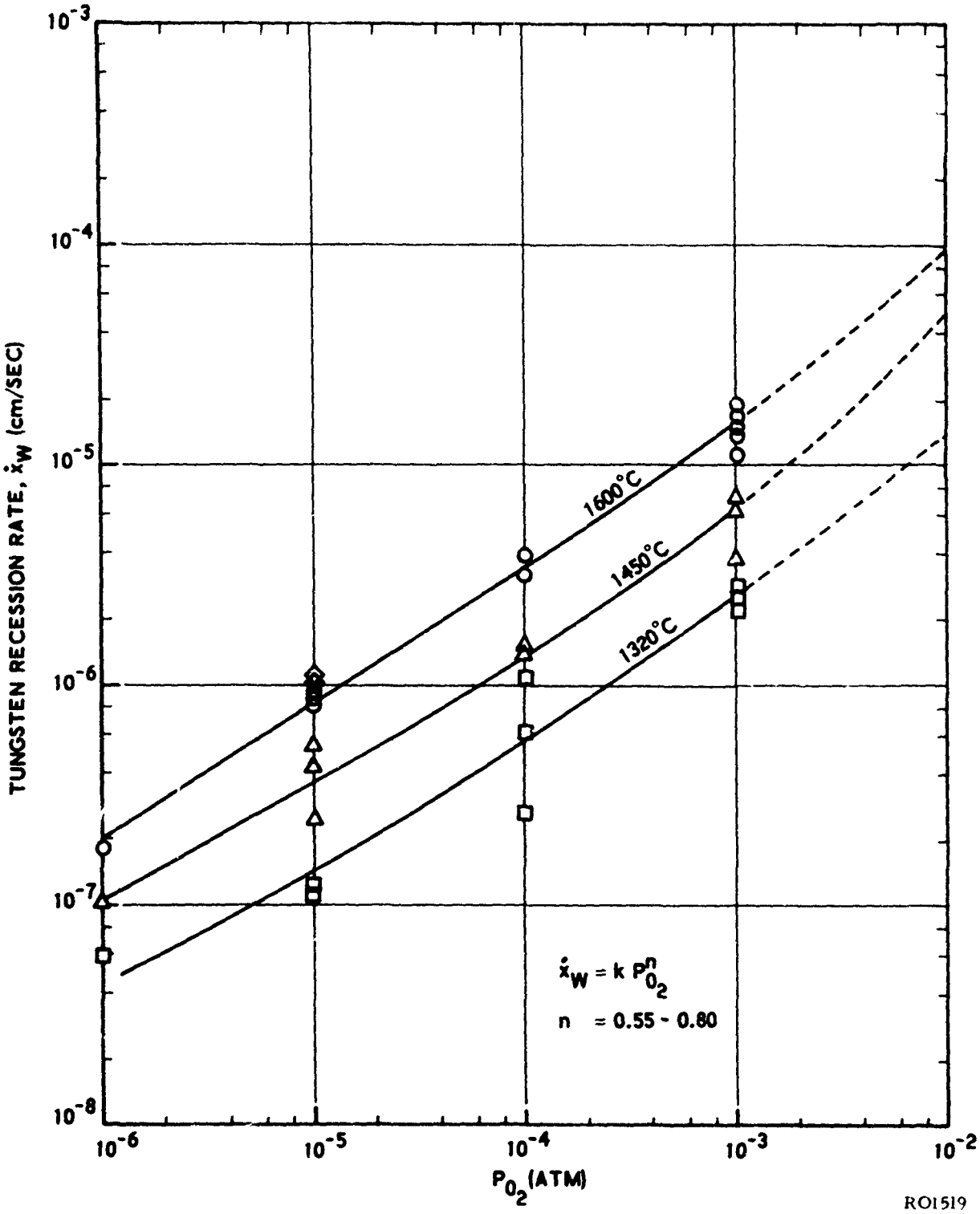

FIGURE 12. TUNGSTEN OXIDATION RATE DEPENDENCE ON P_{O_2} BELOW 2000°C

The temperature and oxygen pressure dependence of the rate below 2000°C was well behaved for pressures of 10^{-2} atm and lower. However, because of the perturbing influence of the gas boundary film, data was analyzed only at 1600°C and lower temperatures and 10^{-3} atm and lower oxygen pressures. For these conditions $P_{O_2(s)} \simeq P_{O_2\infty}$. The pressure dependence, $P_{O_2}^{n}$, shown in Figure 12 at three temperatures, varies between n = 0.55 and n = 0.80 and increases with pressure. A straight line fit was made for the low temperature sections of each of the isobars, 10^{-6} atm through 10^{-3} atm inclusive, of Figure 6. The average value for the experimental activation energy, E_a, was 42 Kcal/mole and gave the following empirical rate equation for temperatures below 2000°C:

$$\dot{X}_W(\text{cm/sec}) = (7 \times 10^6) \; P_{O_2}^{2/3} \; \exp(-E_a/RT) \qquad (12)$$

6. DISCUSSION OF THE MECHANISM FOR OXIDATION AT HIGH TEMPERATURES

The adsorption of oxygen on tungsten has been studied by J. A. Becker[35] and J. Eisinger[14] using Bayard Alpert ion gauge pressure measuring techniques at pressures lower than those of this investigation. The results obtained after heating tungsten at very low pressures to remove adsorbed oxygen followed by quenching to 300°K indicate that oxygen is chemisorbed in two or three successive states with the total adsorption equivalent to two complete monolayers of oxygen atoms. Becker has also shown that the oxygen is removed in two different temperature ranges giving further credence to the two monolayer theory. For purposes of this discussion, the term monolayer is taken to represent different states of adsorbate binding, probably caused by differences in coordination number. The sticking probability, S, defined as the fraction of those oxygen molecules that chemisorb to those that arrive, is plotted in Figure 13. Both investigators observe that the sticking probability changes rapidly after each monolayer is completed.

The results of the present study show that after making the proper convection corrections, a constant value of the reaction probability, $\epsilon = 0.06$, can account for the oxidation of tungsten above 2000°C at all pressures between 10^{-6} atm and 1 atm. This value of ϵ lies between the two values reported for the second monolayer sticking probability, S_2. This correlation suggests that at pressures above 10^{-6} atm, the first monolayer is completely covered, $\theta_1 = 1$, at all temperatures and that above 2000°C, chemisorption of oxygen in the second monolayer results in immediate reaction and evaporation of a tungsten oxide molecule in a non-activated process. According to Berkowitz, et al.[30], the favored molecule produced above 2000°C is $WO_2(g)$. These conclusions indicate the following reaction sequence at the tungsten surface:

$$W + \tfrac{1}{2} O_2 \underset{}{\overset{K_1}{\rightleftharpoons}} W - O \qquad (13)$$

s s

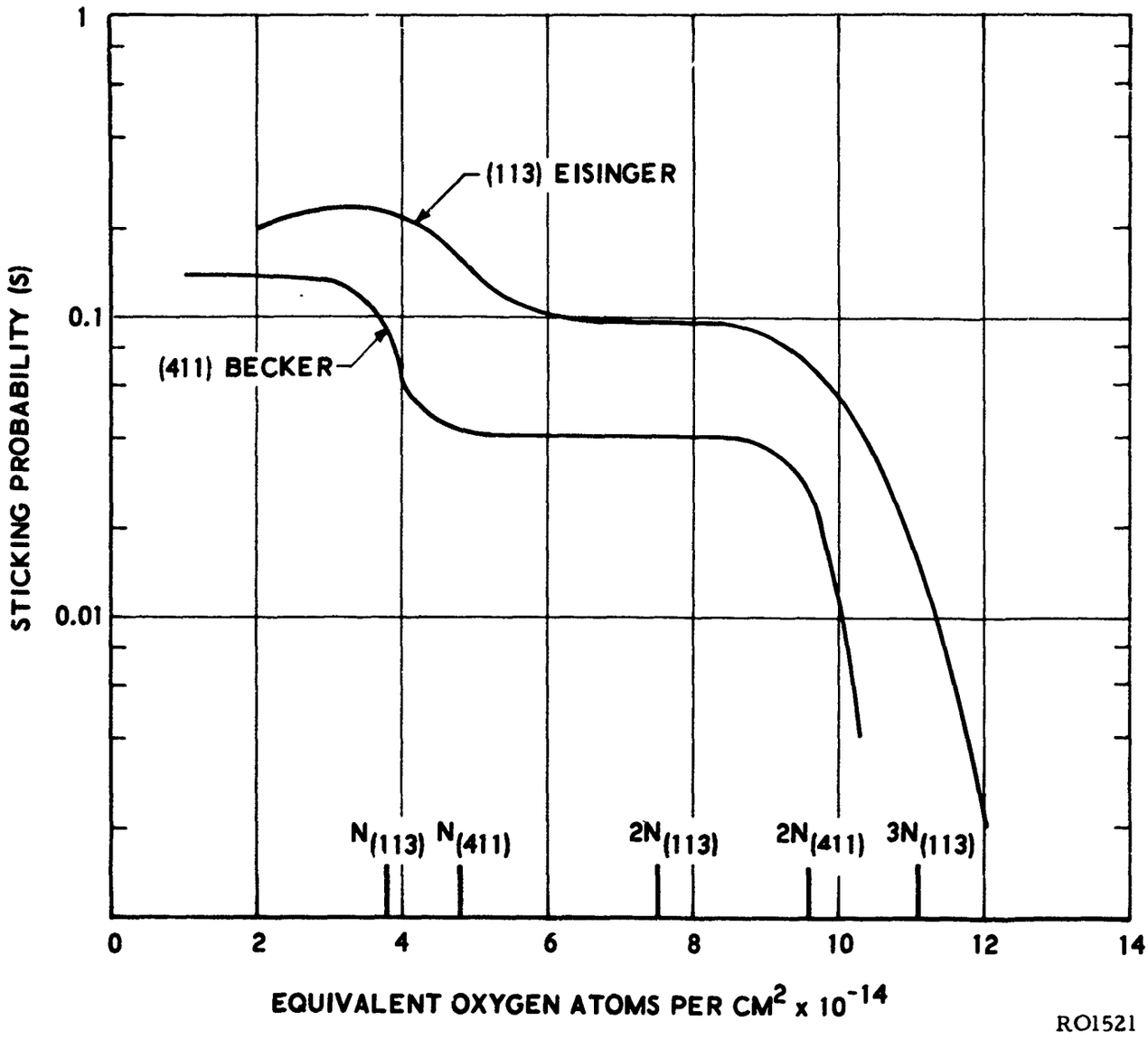

FIGURE 13. STICKING PROBABILITY OF OXYGEN ON (113), REF. 14, AND (411), REF. 35 TUNGSTEN PLANES; TUNGSTEN ATOM CONCENTRATION INDICATED

$$\underset{s}{|}W - O + O_2 \longrightarrow WO_{2(g)} + \underset{s}{\|}W - O \qquad (14)$$

where $\underset{s}{\|}W$ represents a bare surface site for adsorption in the first monolayer and $\underset{s}{|}W - O$ represents a covered site. The rate is:

$$\text{Rate} = (S_2\,\theta_1)\;\nu_o\;P_{O_{2(s)}} \qquad (15)$$

The oxidation data below 10^{-6} atm indicates a decrease in ϵ with decreasing P_{O_2} and increasing temperature. This is not inconsistent with the preceding model but it does confirm that surface coverage of the first monolayer decreases, since $\epsilon = S_2\,\theta_1$, and suggests that θ_1 conforms to a Langmuir adsorption equation with a proper negative value for the adsorption enthalpy.

$$\theta_1 = \frac{K_1\,P_{O_2}^{\frac{1}{2}}}{1 + K_1\,P_{O_2}^{\frac{1}{2}}} \qquad (16)$$

The data[14-16] are insufficient to permit an accurate determination of ΔH_1.

Anderson's value for ϵ at 10^{-6} atm and 2000°C is 0.035, based on formation of WO_2, and changes very slightly with temperature[16]. Langmuir's data[13] taken at 2.6×10^{-7} to 6×10^{-5} atm does not show a decrease in ϵ and the value is about the same as determined in the present investigation.

Now consider the results below about 2000°C. At pressures to 10^{-2} atm, the limit of the present study, the rate of oxidation is less than $S_2 \nu_o P_{O_{2(s)}}$ and, therefore, partial surface coverage of the second monolayer probably occurs, $0 < \theta_2 \ll 1$. If one chemisorbed atom from each of the first and second monolayers is required for the formation of $WO_{2(g)}$, by an activated process, then the rate of WO_2 formation becomes proportional to θ_2 which gives a half power oxygen pressure dependence ($P_{O_2}^{\frac{1}{2}}$) for low values of θ_2. Based on the similar premise that the formation of $WO_{3(g)}$ requires two chemisorbed atoms from the second monolayer and one chemisorbed atom from the first monolayer, the WO_3 formation rate should be proportional to $(\theta_2)^2$, giving a first power oxygen pressure dependence (P_{O_2}) for low values of θ_2. These process steps are summarized below:

$$\underset{s}{|}W - O + \tfrac{1}{2}\,O_2 \underset{}{\overset{K_2}{\rightleftharpoons}} \underset{s}{W\begin{smallmatrix}O\\O\end{smallmatrix}} \qquad (17)$$

$$\theta_2 \simeq K_2 P_{O_2}^{\frac{1}{2}} \qquad (\theta_2 \ll 1) \tag{18}$$

$$\underset{s}{\left| W \begin{smallmatrix} O \\ \diagup \\ \diagdown \\ O \end{smallmatrix}\right.} \xrightarrow{k'} WO_{2(g)} \tag{19}$$

$$\text{Rate}_{(WO_2)} = N_o \theta_2 k' \tag{20}$$

$$2 \underset{s}{W \begin{smallmatrix} O \\ \diagup \\ \diagdown \\ O \end{smallmatrix}} \xrightarrow{k''} WO_{3(g)} + \underset{s}{W - O} \tag{21}$$

$$\text{Rate}_{(WO_3)} = N_o^2 (\theta_2)^2 k'' \tag{22}$$

The mass spectrometric data of Berkowitz, et al.[30], indicates that approximately equal amounts of WO_2 and WO_3 are formed below 2000°C at 10^{-6} atm. This should give a pressure dependence for the recession rate of about $P_{O_2}^{0.75}$ at this pressure, in agreement with Figure 12. With increasing pressure, the rate of formation of WO_3 will increase faster than that of WO_2 because of its higher pressure dependence. Therefore, the over-all pressure dependence of the recession rate should increase with increasing pressure, also in agreement with Figure 12.

7. SUMMARY OF FINDINGS

The results showing tungsten oxidation rates as surface recession rates at a variety of temperatures and pressures are summarized in Figure 6. At the oxygen pressures of interest for earth atmosphere reentry, above 10^{-6} atm, there is no significant increase or decrease in the rate above 2000°C. Below 2000°C, an exponential temperature dependence typical of chemical kinetic processes is encountered. The oxidation rates are affected by the gas boundary film adjacent to the surface. The actual rates of oxidation under reentry conditions will be greater than the experimentally measured rates at equivalent ambient oxygen pressures because of highly forced convective transfer of oxygen to the surface rather than free convection conditions encountered in these experiments. However, the recession rates can be calculated if the appropriate surface temperatures, oxygen stagnation pressures, free stream velocities and boundary film correlations for the forced convective condition are used in conjunction with the surface recession rate of equation (4), using $\epsilon = 0.06$. This topic will be pursued in the next section.

SECTION 2

OXIDATION OF POLYCRYSTALLINE TUNGSTEN IN A HYPERSONIC GAS STREAM

The data obtained from oxidation of polycrystalline tungsten rods and summarized in the previous section has shown that at high temperatures and oxygen pressures above 10^{-5} atm, transport of oxygen through the adjacent boundary film, formed by the oxide product vapor species, limits the rate of oxidation. Furthermore, inert gas (argon) present in the boundary film severely retards the oxidation rate. These findings suggested that the oxidation rate should increase in a forced convective oxidizing environment. They also suggested that an artificial source of inert gas near the boundary film might reduce the rate of oxidation of tungsten and permit employment of tungsten structures at high temperatures in oxidizing atmospheres for limited periods. Consequently, experiments were conducted in oxygen-argon mixtures flowing over polycrystalline tungsten rods at hypersonic velocities.

1. EXPERIMENTAL

The hypersonic flow experiments were performed using a 120 kilowatt D.C. arc plasma re-entry test facility shown in Figure 14. Each tungsten test rod was inserted in the test chamber with its axis normal to the gas flow. An argon plasma was generated into which oxygen was injected upstream from the sample. Gas mixtures of 5% and 20% oxygen in argon were employed. The gas velocity forward of the bow shock, caused by impingement of the gas stream on the sample, was 15000 ft/sec. The velocity back of the bow wake, which is the equivalent free stream velocity experienced by the sample boundary film, was estimated to be 3200 ft/sec using normal shock functions for one-dimensional flow after Shapiro[36]. These high velocity conditions required the use of a large evacuated receiving chamber surrounding the sample. The enthalpy of the gas stream was adjusted so that the steady state sample temperatures were $1960^{\circ}C \pm 50$ for the 5% oxygen mixture and $2050^{\circ}C \pm 50$ for the 20% oxygen mixture. These temperatures were measured with a 0.65 μ optical pyrometer. Emissivity corrections were not made, but temperature corrections for window absorptivity were used. Samples were mounted on a swinging arm which permitted rapid insertion of the sample in the hot gas stream after flow conditions were adjusted and rapid removal of the sample after exposure for a precise period of time. Rates were determined by comparing sample diameters measured with a micrometer before and after exposure.

2. OXIDATION RATES IN HYPERSONIC GAS FLOW

As expected from the findings of the previous section, the tungsten recession rate did not vary appreciably between the 5% and 20% oxygen mixtures. There was some oblating of the sample cross section. The maximum tungsten recession rate was $(2.6 \pm 1) \times 10^{-3}$ inches/minute, 1.2×10^{-4} cm/sec. It is interesting to make some crude comparisons between the conditions of this oxidation rate, which is the result of highly forced convective transfer of

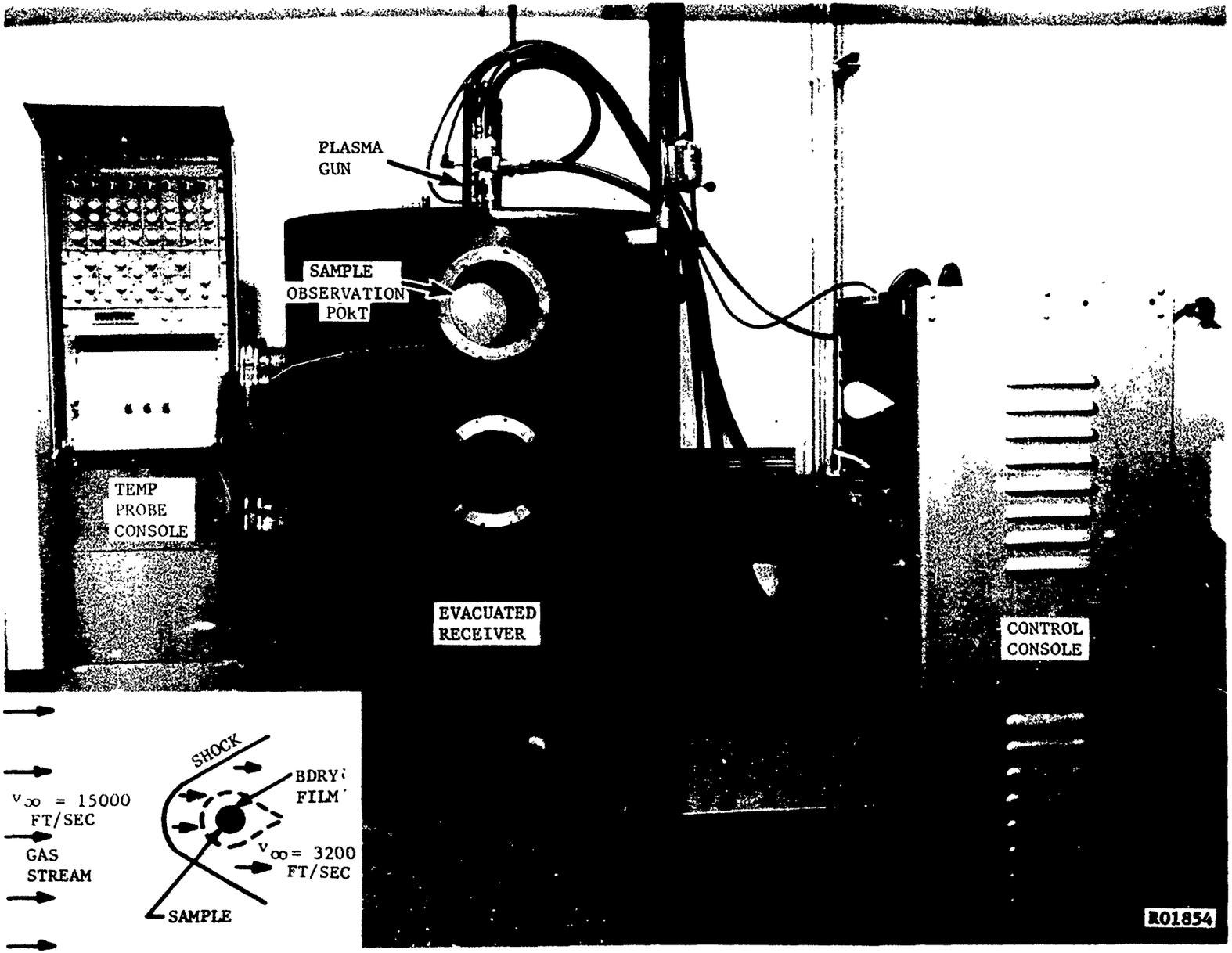

FIGURE 14. 120 KW ARC PLASMA RE-ENTRY TEST FACILITY AND SCHEMATIC OF TUNGSTEN ROD OXIDATION TEST CONDITIONS

oxygen to the tungsten surface, with free convective conditions that provide equivalent recession rates. In pure oxygen, a pressure of only 2 mm Hg is required to sustain this rate under free convective conditions. This is less than the oxygen partial pressure employed in the hypersonic flow tests. This discrepancy, of course, is caused by the argon dilutent present in the boundary film during the hypersonic flow tests. An alternate comparison can be made. For a 9 to 1 argon-oxygen mixture, which is between the two mixtures used in the hypersonic flow tests, an oxygen pressure of about 75 mm Hg and a total pressure of about one atm. would be required under free convection. See Figures 6 and 10. This is substantially higher than the actual stagnation pressures, measured by a Pitot tube, in the hypersonic flow tests which were $0.13 \pm .02$ atm. Thus, the experimental results confirm that a lower total pressure, stagnation pressure, is required under forced convection to obtain the same recession rate obtained under free convection when equivalent gas mixture ratios are compared. This approach was carried one step further by predicting the oxidation rates using dimensionless parameter correlations for forced convection about a cylinder transverse to the stream. The Chilton-Colburn mass transport dimensionless group analogy for the heat transport dimensionless group, $j_D = j_H$, was used[37];

$$\text{where } j_D = Nu_{AB} Re^{-1} Sc^{-1/3} \tag{23}$$

$$\text{and } j_H = Nu\ Re^{-1} Pr^{-1/3} \tag{24}$$

The correlation for heat transfer published by Sherwood and Pigford[38] was used to calculate the forced convection mass transfer coefficient, k_m. This correlation, for mass transfer, is shown in Figure 15. The dimensionless group, j_D, is plotted against the Reynolds number, Re. For the sample diameter, effective free stream velocity, and stagnation pressure used in the hypersonic flow tests the Reynolds number is 2.8×10^4. From Figure 15, the corresponding value of j_D is 4.3×10^{-3}. From the previously mentioned data and the effective gas temperature, 2400°K, the diffusivity D_{AB}, gas viscosity μ_g, and density $\bar{\rho}$ were calculated using equations (10) and (11) and the perfect gas law. The mass transfer coefficient was calculated from the value of j_D and the values of the other parameters comprising j_D. For the hypersonic test conditions $k_m = 2.1 \times 10^{-4}$ moles $cm^{-2} sec^{-1}$. Using equations (4) and (5) the following equation identical in form with equation (9) was derived and used to calculate the oxidation rate under these conditions:

$$\dot{x}_w = \frac{\epsilon \nu_o P_{O_2}}{1 + \frac{\epsilon \nu_o P_t}{k_m (M_w / \rho_w)}} \tag{25}$$

The calculated and experimental results are compared in Table II. Calculated and experimental results for free convection at identical argon and oxygen

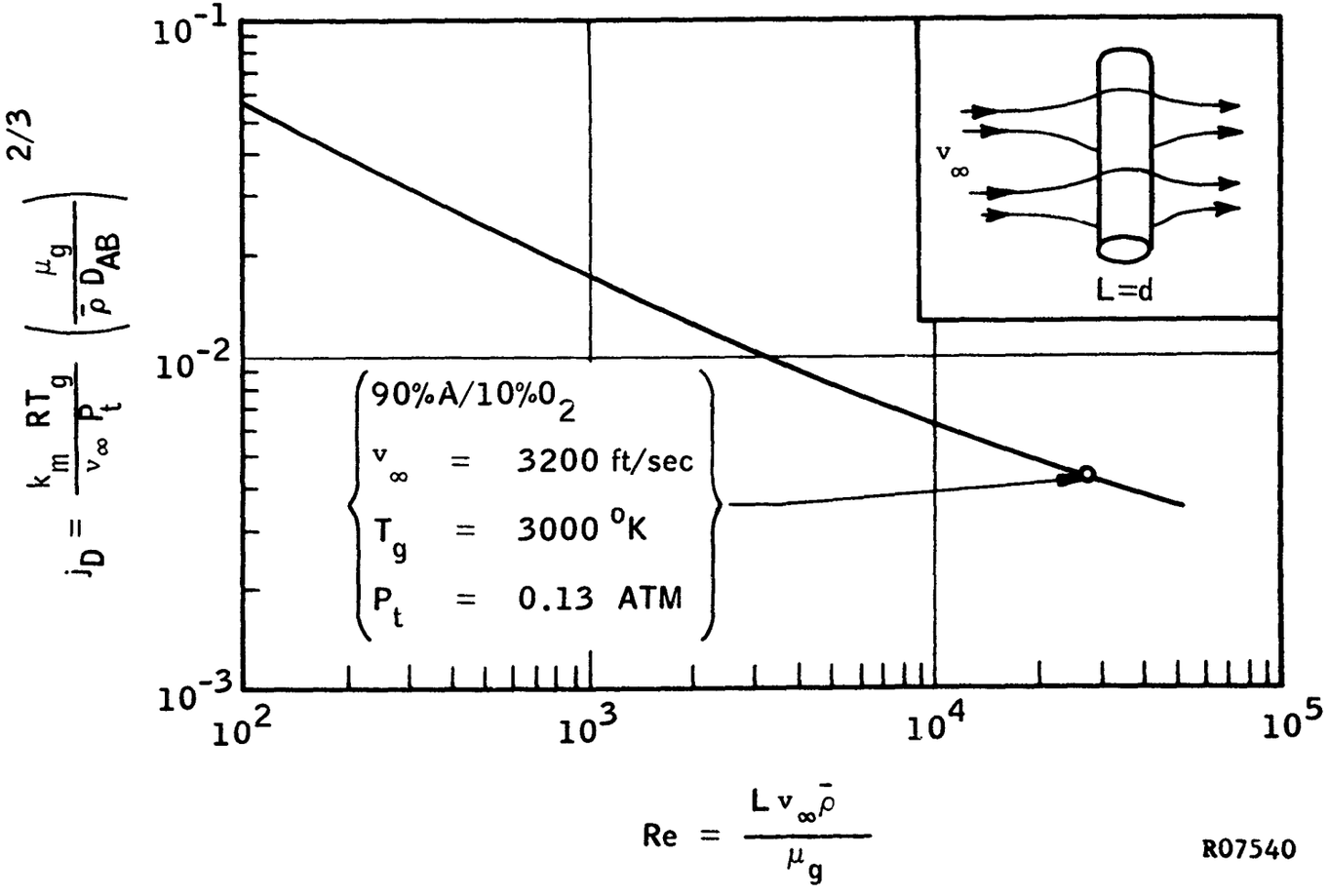

FIGURE 15. FORCED CONVECTION CORRELATION FOR CYLINDERS, CHARACTERISTIC LENGTH L EQUALS DIAMETER d

pressures are also compared. In both cases, calculated and experimental results are in excellent agreement. Hypersonic flow increases the oxidation rate five or six times over the free convection rate.

TABLE 2

CALCULATED AND EXPERIMENTAL RESULTS FOR OXIDATION OF TUNGSTEN IN AN OXYGEN ARGON ENVIRONMENT AT 2000°C WITH
(a) FREE CONVECTION AND
(b) FORCED CONVECTION IN A HYPERSONIC STREAM

	Free Convection	Forced Convection
Recession Rate	T = 300K T_g = 1350K P_t = 0.13 atm P_{O_2} = 0.013 atm	v_∞ = 3200 ft/sec T_g = 2400K P_t = 0.13 atm P_{O_2} = 0.013 atm
Calculated (cm/sec) x 10^5	2.5	17
Experimental (cm/sec) x 10^5	3.0 ± 1	12 ± 4

3. ABLATIVE COATINGS IN HYPERSONIC GAS FLOW

Limited tests with ablative coatings were unsuccessful. A high temperature phenolic resin* was applied to tungsten rods and cured at 325°F. Upon heating, these coatings were expected to pyrolize and give some protection from both the condensed phase pyrolysis product and the ablating vapor species. An initial oxidation experiment was performed in the rod recession oxidation apparatus at 10^{-2} atm oxygen pressure. The coating quickly flaked off the sample. It was assumed that this was because the source of the heat flux to the coating was from within the sample and that pyrolysis started at the tungsten-phenolic interface rather than at the oxygen interface Subsequent tests were performed in the re-entry test facility, but the results were not significantly different. The coating flaked off within 3 to 7 seconds before the steady state sample temperature was reached.

---

* Cincinnati Testing Laboratory 91LD

4. SUMMARY

Forced convective oxidation experiments were performed using argon-oxygen mixtures heated by an arc plasma and flowing at hypersonic velocities. For the test conditions, the oxidation rate was increased five to six times over the rate in a free convective environment at the same oxygen and argon pressures. The experimental rates were in excellent agreement with predicted rates calculated from dimensionless parameter correlations for transverse flow over cylinders. These results provide further evidence of the importance of oxygen transport through the boundary film adjacent to the sample.

Tests using thin organic ablative coatings to reduce oxidation rates were unsuccessful. Nevertheless, the principal of injecting a nonoxidizing gas into the boundary film is a sound approach for markedly lowering the oxidation rate provided a practical injection method can be developed. Injection through a porous tungsten wall is an attractive approach to this problem.

SECTION 3

THE INFLUENCE OF CRYSTAL ORIENTATION ON THE OXIDATION OF TUNGSTEN

A study of the effect of metal crystal orientation on oxidation rates at temperatures where condensed oxides form has been made for tungsten[39] and several other metals[40]. Similar studies at high temperatures where the oxide products vaporize are rare in general and have not been made for tungsten. The purposes of the study reported in this section were to investigate variations in the oxygen reaction probability, ϵ , used in equation (4) of Section 1 during oxidation of different low index faces of tungsten. Observations of the tungsten surface morphology following oxidation were also made.

1. EXPERIMENTAL

One half inch diameter single crystals of known [hkl] orientation were cut to expose parallel (hkl) faces. Using a 2% NaOH electrolyte, these surfaces were electropolished and some were electroetched to develop etch marks and to outline subgrain boundaries. The oxidation procedure is described below. Samples were set on a thin tungsten pedestal located in a vacuum chamber, Figure 16. A stable mounting was accomplished using an insertion hole drilled in the side of the sample. The chamber was evacuated and backfilled with dry oxygen to 1×10^{-6} atm. This particular oxygen pressure was chosen and used exclusively because of several advantages. First, this pressure was high enough to permit removal of considerable tungsten. This allows full development of morphological changes and insures accurate rate measurements. Second, although this pressure is higher than typical condensation-evaporation experiments in metal systems, it is lower than required to form a gas boundary film sufficient to effect the rate of oxidation. Third, at this pressure, there is comparative rate data for polycrystalline tungsten from the current studies, Section 1, and Anderson's data[16]. All samples were oxidized at 2050°C ± 50°C using an R.F. induction coil. Temperature was measured with a calibrated disappearing filament pyrometer using corrections for the emissivity of tungsten and calibrated window absorptivity. The oxidation rate was determined by measuring the decrease in distance between parallel faces.

The tungsten crystals used as samples were grown by the Linde Company using a plasma arc Verneuil technique, Table 3. In all cases, misorientation of crystal faces with the surface was less than 5 degrees.

Since the orientation and appearance of etch pits and hillocks generated in aqueous solutions were used to correlate the morphological results of high temperature oxidation, a brief introductory discussion of wet etch marks on tungsten is necessary. Etch pits in tungsten have been studied extensively by Schadler[41] using a $CuSO_4 \cdot NH_4OH$ solution and by Berlec[42] using both a $CuSO_4 \cdot NH_4OH$ solution and a 2% NaOH solution. The results using either etchant are identical. Square etch pits are developed on (100) surfaces and elongated triangular pits develop on (112) surfaces of tungsten. In both cases, the defining sides of the

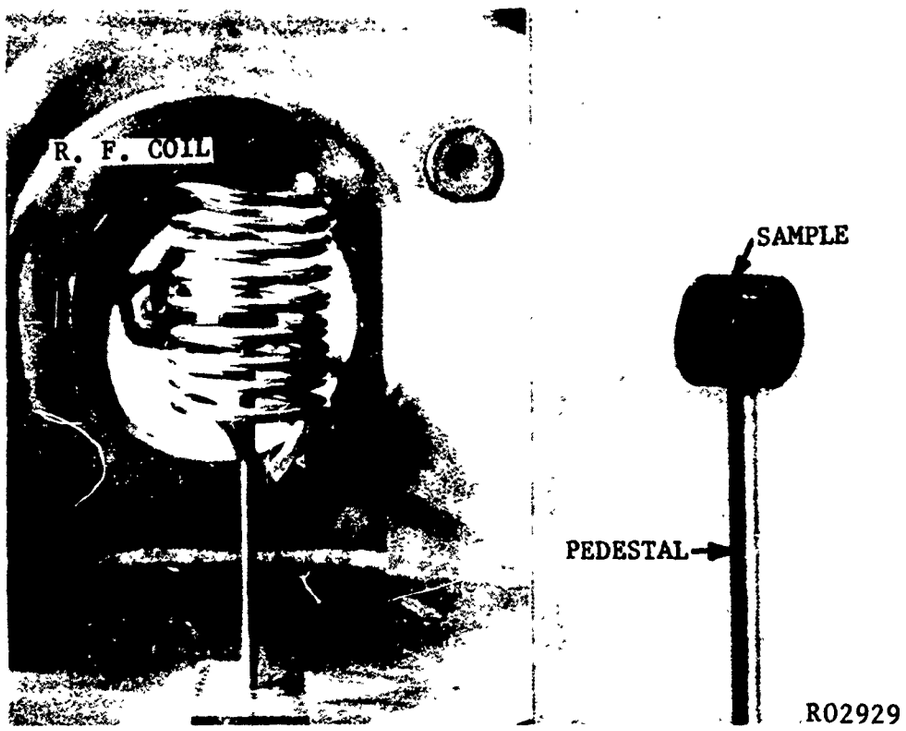

FIGURE 16. "LOLLIPOP" SETUP FOR OXIDIZING TUNGSTEN SINGLE CRYSTALS

etch pits are {110} planes. Plastic deformation and matched etch pit patterns in cleaved surfaces indicate that the etch pits coincide with dislocations intersecting the surface. Berlec[42] has observed small oriented etch hillocks with a triangular outline on heavily etched (111) surfaces of tungsten. Neither etch pits nor hillocks occur on (110) surfaces of tungsten. All of these results were confirmed during the present study. We have also found that the wet etch pyramids on (111) surfaces do cluster at subgrain boundaries, suggesting an association with dislocations.

TABLE 3

NOMINAL COMPOSITION TUNGSTEN CRYSTALS

C	6 ppm	Fe	0.01%
O	5 ppm	Mg	0.001
Al	0.01 %	Mn	0.01
Co	0.003	Mo	0.1
Cu	0.001	Ni	0.01
Cr	0.01	Si	0.01

2. RESULTS

The measured values for reaction probabilities on (100), (110), and (111) faces are shown in Table 4. These data are also shown in graphical form and compared with polycrystalline data at the same pressures in Figure 17. The values for (110) and (111) faces are similar to the polycrystalline values; but the reaction probability on the (100) face was much faster, $\gamma = 0.41$.

The differences in morphology of the tungsten surface were more striking, but the results were equally reproducible. Polished (100) and (111) surfaces tended to remain smooth while (110) surfaces were jagged. Grooving of subgrain boundaries occurs on (100) and (111) surfaces. Etch pits or other indications of accelerated oxidation at dislocations were not observed on any of the crystal faces as a result of oxidation. Wet etch pits introduced before oxidation lost definition as a result of oxidation but did not change otherwise. The series of micrographs in Figure 18 show this effect on a (100) surface. The initial etch pits are 10 microns across. They are concentrated at subgrain boundaries and distributed randomly within grains. The large diamond shaped marks are hardness indentations used to relocate areas after oxidation. After 10 minutes the surface has receded 11 microns, approximately the width of the wet etch pits. The bottoms of the pits are flat rather than pointed, and

TABLE 4

MEASURED REACTION PROBABILITIES BASED ON
AN OXIDATION PERIOD OF 420 MINUTES AT 2050°C AND: $W + O_2 \rightarrow WO_2(g)$

$P_{O_2} = 1 \times 10^{-6}$ Atm, T = 300°K; $\epsilon = \text{Rate}_{(cm/sec)} \left(\frac{\rho_W N_O}{M_W P_{O_2}}\right) (2\pi mkT)^{\frac{1}{2}}$;

$$\epsilon = 9.84 \times 10^{3} \text{ Rate}_{(in/min)}$$

Sample	Face	Avg. Face Recession	Recession Rate (in/min)	ϵ
W-12	(100)	0.0176	4.2×10^{-5}	.41
W-13	(100)	0.0172	4.1×10^{-5}	.40
W-20	(100)	0.0186	4.3×10^{-5}	.42
W-4	(110)	0.0032	7.7×10^{-6}	.076
W-7	(110)	0.0032	7.6×10^{-6}	.075
W-8	(110)	0.00295	7.0×10^{-6}	.069
W-31	(111)	0.0040	9.5×10^{-6}	.093
W-32	(111)	0.0040	9.5×10^{-6}	.093
W-33	(111)	0.00395	9.4×10^{-6}	.092

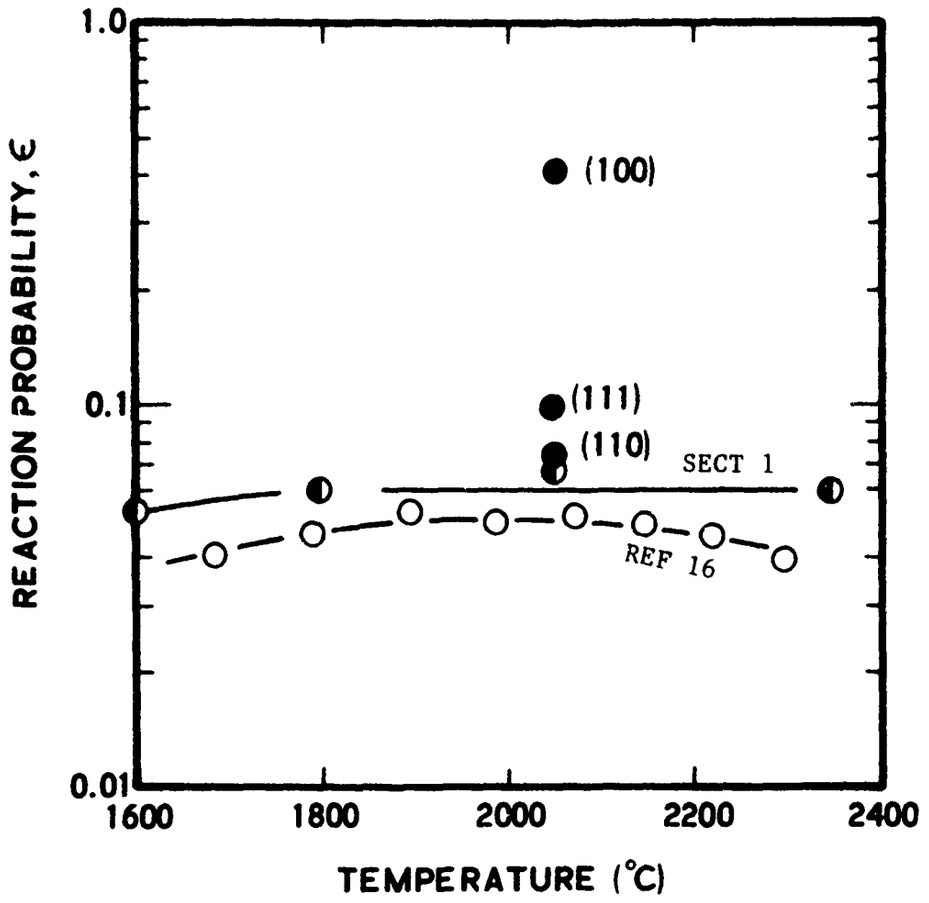

205848

FIGURE 17. REACTION PROBABILITY FOR POLYCRYSTALLINE TUNGSTEN WIRE[4] AND ROD[7] AND SINGLE CRYSTAL LOW INDEX FACES AT 1×10^{-6} ATMOSPHERES OXYGEN PRESSURE

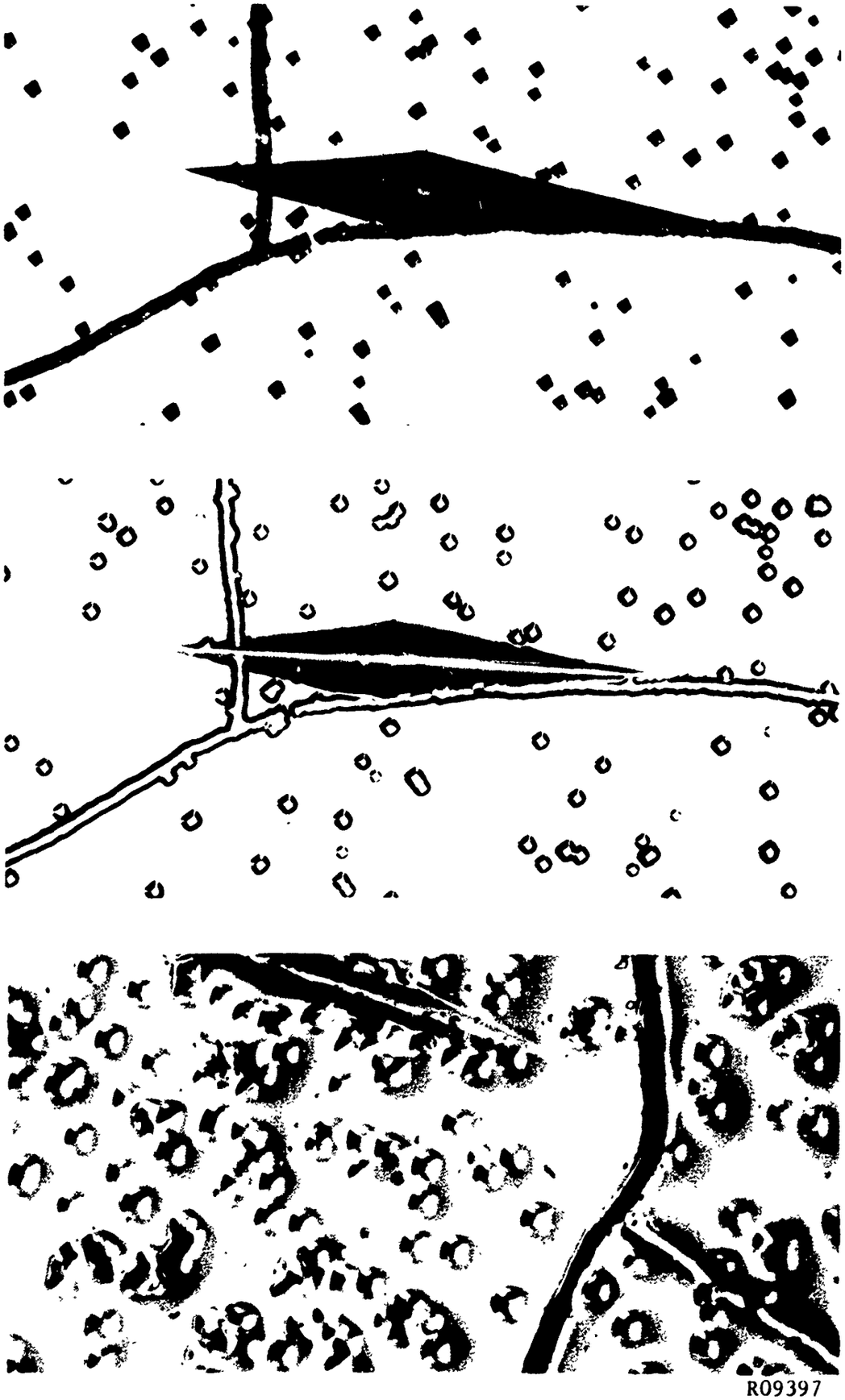

FIGURE 18. EFFECT OF OXIDATION ON DISLOCATION ETCH PITS INTRODUCED PREVIOUSLY BY ELECTROLYTIC ETCHING IN 2% NaOH SOLUTION; OXIDATION AT 2050° C, 375X

there is some rounding of corners and edges. After 90 minutes of oxidizing to a depth approximately ten times the original wet etch pit diameter, evidence of the pit is still present but the pit outlines are very obscure.

A. (100) Surface

Examination of the 90 minute oxidation micrographs reveals occasional marks similar to the wet etch pits. These marks are the initial appearance of growth anomalies on (100) surfaces which remain for extended periods of oxidation and eventually become octahedral pyramids. These growth forms also appear as small rounded craters in their early stages. Sometimes they appear as shallow polyp structures containing fourfold symmetry. A mature octahedral pyramid is shown in Figure 19. It is considerably larger than a wet etch pit. Its sides are bound by {111} faces rather than the {110} faces observed for wet etch pits. The octahedral faces are stepped to provide for a flatter total pyramid shape without sacrificing the exposure of low index phases at the surface. However, the edges of each pyramid, where the {111} planes intersect, are not stepped. This leads to the fourfold appearance of inverted rings shown in Figure 19. The stepped pyramid structure is more readily seen in a carbon replica electron micrograph, Figure 20. The details of the edges of these octahedral pyramids are shown in Figure 21. The center of these pyramids may (1) simply be a continuation of the pyramid structure, Figure 20; (2) have the appearance of Figure 19; or (3) contain the fourfold shallow polyps. Two examples of the latter are shown in Figure 22.

The mature stepped pyramid structures are slow to develop. Those shown in Figures 19-22 were formed by an oxidation period of seven hours. There are comparatively few of these structures on the surface, but they were observed on all samples oxidized more than three hours. Usually they are scattered randomly in subgrains, but clusters do occur. They have been seen at subgrain boundaries, but there is no preference for this location. Their orientation is fixed by their {111} faces and the orientation of the crystal. The orientation of several pyramids is shown in the dark field micrograph, Figure 23. Small misorientations between adjacent subgrains are reflected in small changes in orientation of the stepped pyramids contained within them. As with wet etch pits, slight misorientation of the surface with respect to the (100) plane causes distortions of the symmetrical shape of the pyramids.

The octahedral pyramids are not initiated at dislocations, but mature pyramids act as traps for dislocations. A polished (100) surface was oxidized seven hours and later marked with a referencing hardness indentation near two octahedral pyramids. The only features of the resulting micrograph, in addition to the indentation mark and two mature pyramids, are five incipient pyramids in the form of small craters present in the upper right hand corner but difficult to distinguish in the reproduced micrograph, Figure 24.

The sample was subsequently etched in 2% NaOH to develop wet etch pits. This is shown in the second micrograph of Figure 24. Dislocations clustered within the strain hardened area around the indentation mark as expected. However, equally dense dislocation clustering has occurred within the octahedral pyramid. Wet etch pits have not developed on or near the small craters. Because the wet etch pits are bound by {110} faces their outline is rotated 45° with respect to the square outline of the octahedral pyramids.

P05850

FIGURE 19. FLATTENED, STEPPED OCTAHEDRAL PYRAMID ON (100) SURFACE OF TUNGSTEN, 1600X

FIGURE 20. CARBON REPLICA OF STEPPED PYRAMID ON (100) TUNGSTEN SURFACE, 3000X

FIGURE 21. EDGE DETAIL OF OCTAHEDRAL PYRAMID ON THE (100) TUNGSTEN SURFACE SHOWING JUNCTION OF $\{111\}$ FACES OF THE PYRAMID; CARBON REPLICA, 6000X

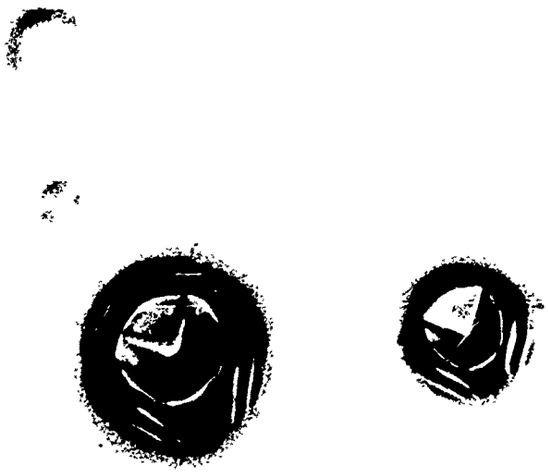

P05853

FIGURE 22. OCTAHEDRAL PYRAMIDS ON (100) SURFACE WITH CORES HAVING THE SHAPE OF SHALLOW POLYPS

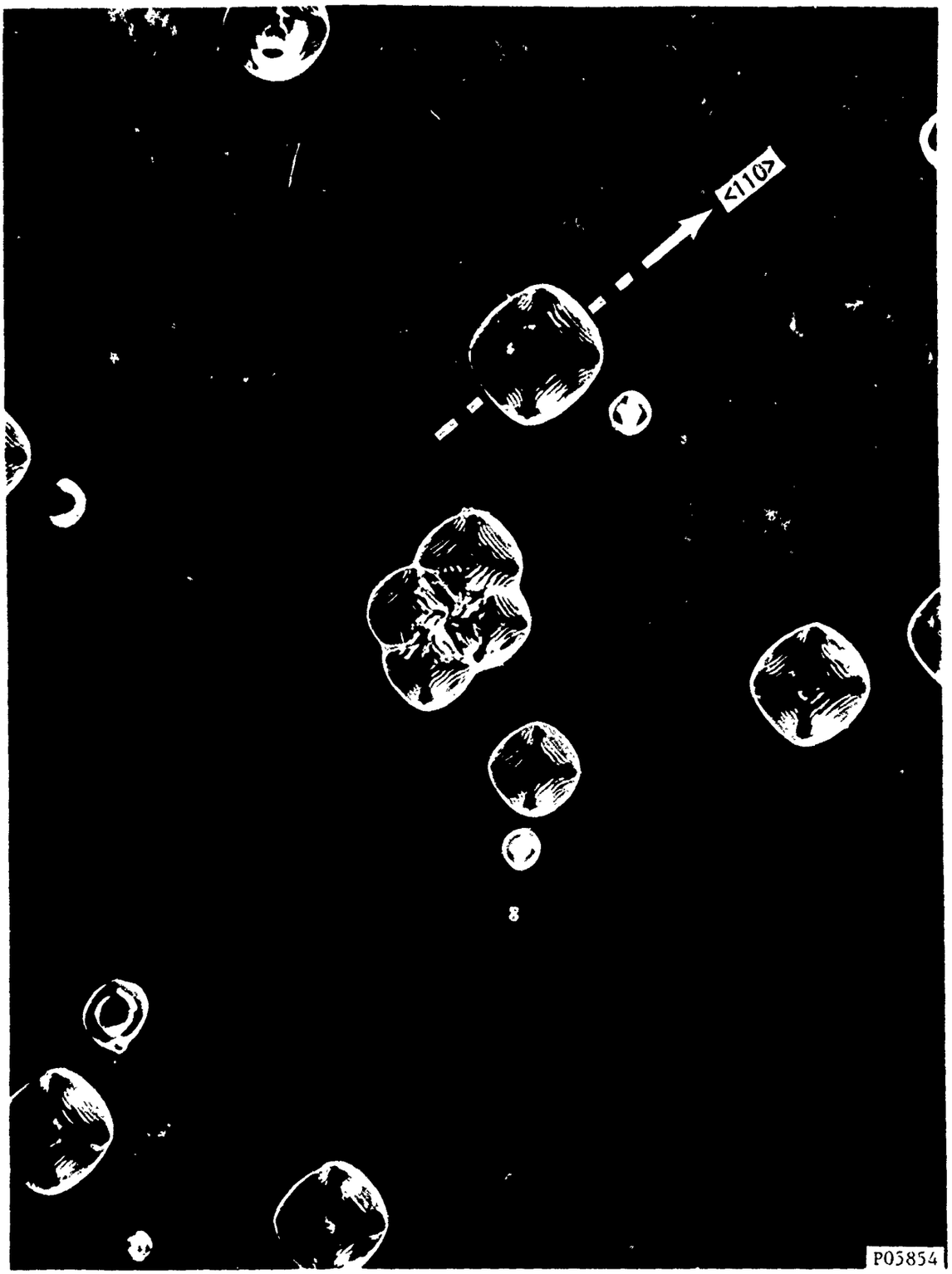

FIGURE 23. ORIENTATION OF STEPPED OCTAHEDRAL PYRAMIDS ON (100) TUNGSTEN SURFACE; DARK FIELD ILLUMINATION, 260X

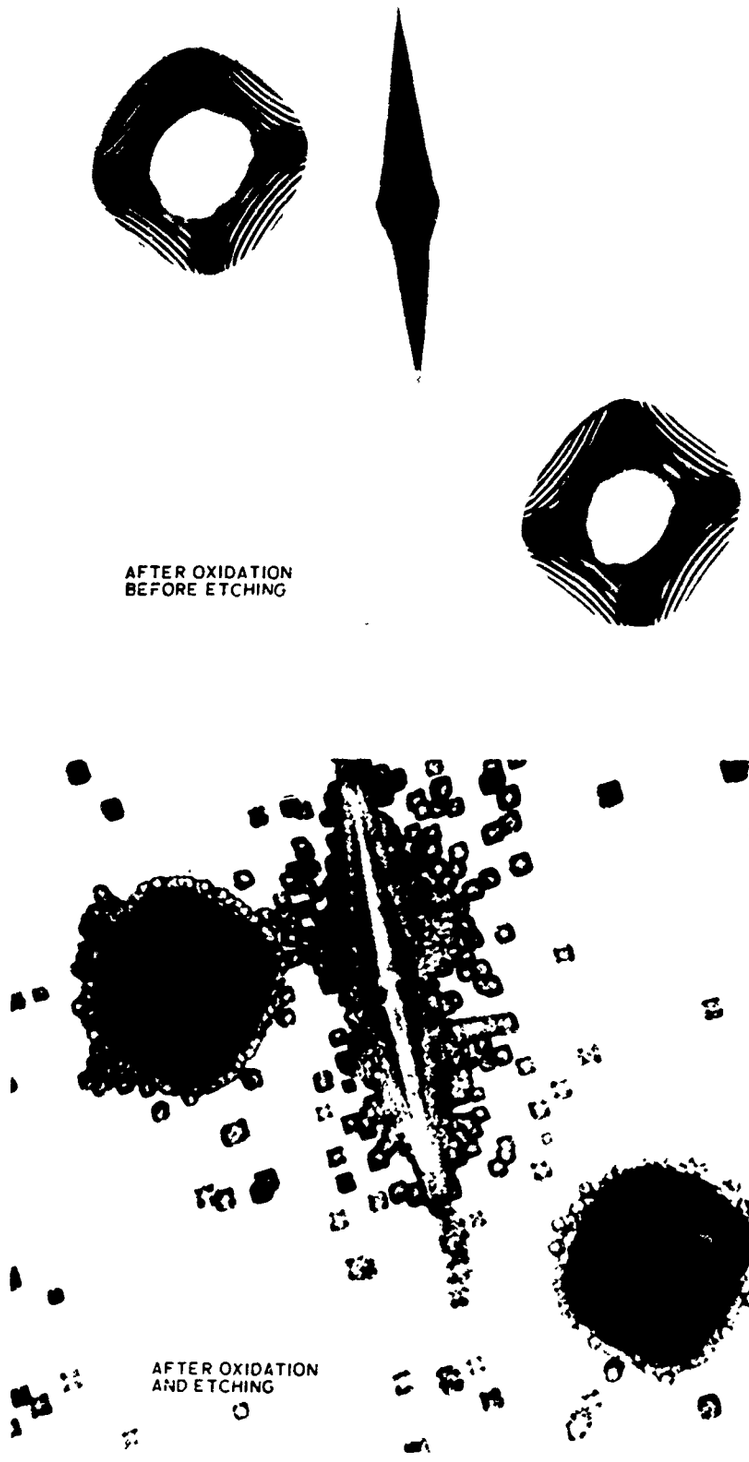

FIGURE 24. POST OXIDATION WET ETCHING TREATMENT SHOWS ACCUMULATION OF DISLOCATIONS AT STEPPED PYRAMIDS ON (100) TUNGSTEN SURFACE, 400X

Electron microprobe analysis of the tungsten surface at the stepped pyramids was undertaken to determine if impurities were influencing this behaviour. Elements other than tungsten were not present in detectable amounts. Furthermore, the tungsten X-ray emission intensity was not diminished at octahedral pyramids relative to the rest of the sample. If tungsten borides, carbides, or nitrides were present as separate phases, a measurable reduction in tungsten X-ray intensity should have been detected.

B. (111) Surface

The morphology development on (111) surfaces was similar to the (100) surfaces. The surface remained smooth, but gradually stepped tetrahedral pyramids matured, Figure 25. They were more numerous than the octahedral pyramids observed on the (100) surface. Electron micrographs show the steps more clearly than light micrographs. In many instances the hillocks are rounded and only approximate tetrahedral shape. These oxidation pyramids are oriented differently than the wet etch pyramids. This is shown in Figure 26. Both micrographs were taken in the same area and identified by hardness indentations, not shown. The sample was wet etched prior to oxidation, left micrograph. The triangles formed by the intersection of the wet etch pyramids with the (111) surface are pointing down and to the left. The results of a one hour oxidation treatment are shown in the right micrograph. A stepped pyramid has formed at the top of the photographed surface, but its triangular outline on the surface is pointing upward and to the right. Oxidation has rounded the wet etch pyramids and is tending to reorient them as triangles pointing in the opposite direction of their original orientation. From a comparison of crystal orientation, as determined from X-ray diffraction studies, with pyramid orientation on the (111) surface we determined that the wet etch pyramids are bound by $\{110\}$ faces while the stepped oxidation pyramids are bound by $\{100\}$ faces. The apparent change in orientation of the wet etch pyramids during high temperature oxidation is caused by the preference for $\{100\}$ faces rather than $\{110\}$ faces under these conditions. Consequently, the $\{100\}$ faces advance and the $\{110\}$ faces recede as defining surfaces for the hillocks.

C. (110) Surface

Pyramids or other definite crystallographic shapes do not form on the (110) surface. Grooving of subgrain boundaries also does not occur although these boundaries usually can be detected and followed in a microscope field because of slight differences in shading which occur at the boundaries. The mature morphology developed after a seven hour oxidation treatment consists of: (1) long serrated ridges; (2) triangular shapes with saw-tooth edges pointing towards shallow depressed areas and all oriented in a common direction; and (3) numerous parallel striations. These are shown in Figure 27. Rare examples of isolated dodecahedral (110) faces can be seen, Figure 28. These occur as small sections of the tungsten crystal projecting outward from the surface.

FIGURE 25. MATURE TETRAHEDRAL PYRAMIDS ON (111) SURFACE OF TUNGSTEN OXIDIZED 7 HOURS AT 2050°C

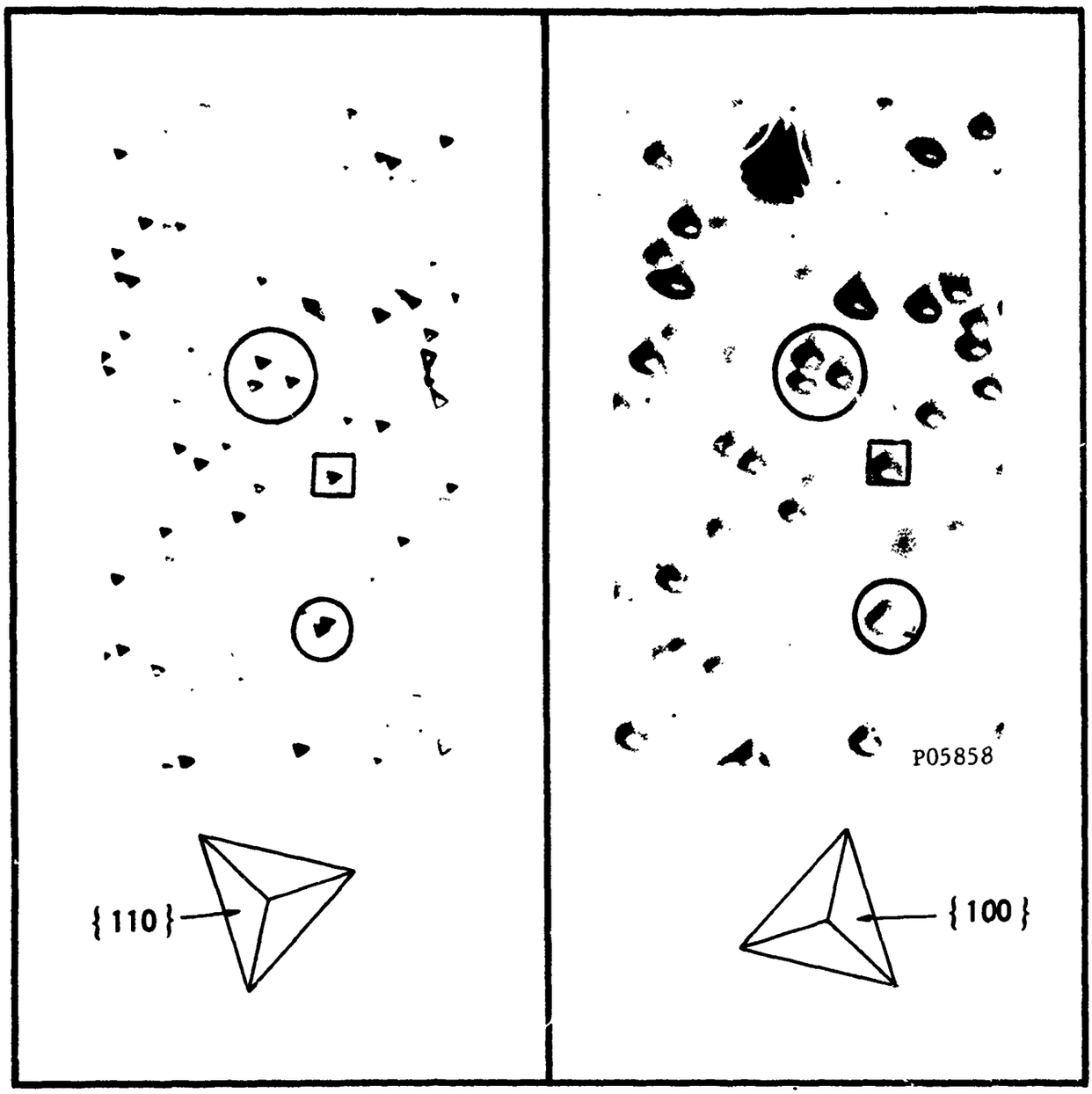

FIGURE 26. ORIENTATION OF WET ETCH PYRAMIDS ON (111) BEFORE OXIDATION

FIGURE 27. CHARACTERISTIC PATTERNS ON THE (100) TUNGSTEN SURFACE RESULTING FROM OXIDATION

FIGURE 28. DODECAHEDREL FACE (DIAMOND SHAPED) PROTRUDING FROM (100) TUNGSTEN SURFACE, 750X

3. DISCUSSION

The results of this study are not easily explained by other published data or models for evaporation and condensation. The order of oxidation rates measured in this study, (100)>(111)>(110) are different from the rates of formation of thin oxide films on tungsten measured by Metrofanov[39] at 400-450°C. The order of the latter study was (111)>(100)>(110), and rate increases were correlated with reductions in electronic work functions. The oxidation mechanisms are different, and agreement is not necessarily expected.

Batterman[43] studied faceted hillocks and pits formed during the etching of germanium in a H_2O_2-HF solution. He reasoned that a stable hillock required that the recession rate of the hillock face be less than the product of the recession rate of the base plane and cosine of their angle of intersection. Batterman's results were generally consistent with this rule but not consistent in all cases. The prevalent formation of tetrahedral pyramids with {100} faces on a (111) base plane of tungsten does not conform with Batterman's rule.

Sticking coefficients of diatomic molecules have been attributed to entropy decreases involved in transforming from the gas phase to the chemisorbed state. In particular, hindered rotation of the molecule in the chemisorbed state appears to be a plausible cause of a sticking coefficient less than unity[45]. On this basis, the sticking coefficient is the ratio of the partition functions for the chemisorbed state and gas state. Since vibration frequencies cannot be evaluated, the approximation that vibrational partition functions have values of unity is taken, and the sticking coefficient is reduced to the reciprocal of the rotational partition function for oxygen

$$\epsilon = \frac{\sigma h^2}{8\pi^2 I k T} \qquad (26)$$

The calculated value for ϵ at 300°K is 0.014. This does not conform with the experimental results, and the model fails to account for the observed rate anisotropy.

When entropy effects are absent, evaporation coefficients are expected to be high and macroscopic ledges absent unless impurities are present[46]. Impurities may be contributing to the observed morphologies, but without positive evidence no conclusions can be drawn.

4. SUMMARY

The oxidation of tungsten at high temperatures was described in terms of moderate deviations from gas collision theory (Hertz Knudsen equation) in Section 1. The probability that a colliding oxygen molecule will react with tungsten is strongly dependent on the crystal face exposed. Of the faces examined, (100) surfaces oxidize most rapidly with a reaction probability approaching unity (0.53). The morphology of oxidized (100) surfaces is smooth with the exception of occasional stepped octahedral pyramids bound by {111} faces. The morphology of (111) surfaces is smooth except for numerous stepped

tetrahedral pyramids bound by $\{100\}$ faces. Initiation of these shapes is not associated with dislocations or detectable impurities. However, dislocations subsequently cluster at mature octahedral pyramids. The morphology of oxidized (110) tungsten surfaces consists of extremely irregular surfaces and macroscopic ledges, but shapes clearly related to crystal geometry were not identified.

SECTION 4

OXIDATION KINETICS OF POLYCRYSTALLINE MOLYBDENUM

The study of molybdenum oxidation rates paralleled the study of tungsten. Identically sized polycrystalline rods, 1/8 inch x 6 inches, were used. The experimental apparatus and procedure were also identical with that described in Section 1. The effects on the oxidation rate of an inert gas mixed with oxygen or forced convection were not investigated, but the oxygen transport through the gas boundary film adjacent to molybdenum is believed to affect its oxidation rate in a manner similar to the oxidation of tungsten. The role of molybdenum crystal orientation was not studied. However, faceting of polycrystalline molybdenum rods during oxidation inferred differences in rates with different crystal faces similar to those for tungsten.

1. RESULTS

Recession rate measurements were made at approximately seven equal increments of reciprocal temperatures between 1380°C (2516°F) and 2470°C (4478°F) and at oxygen pressure decades between 1×10^{-6} atm (7.6×10^{-4} Torr) and 1 atm (760 Torr). A linear rate law was obeyed; e.g., the rate at a fixed temperature and pressure was invariant with time. An Arrhenius plot of the recession rates is shown in Figure 29. Evaporation rates at a total pressure below 1×10^{-7} atm were measured and are shown in the lower left-hand corner of Figure 29. These data show that evaporation of molybdenum is not affecting the oxidation rates shown in the remainder of the graph.

X-ray diffraction analysis of several samples of the residual oxide powder indicates MoO_3 to be the principal constitutent. Variable amounts of Mo_9O_{26} below 30% were also present in these samples.

The oxidation behaviour of molybdenum at high temperatures parallels the oxidation behaviour of tungsten. The rate has an exponential temperature dependence at lower temperatures. Above 1700°C the oxidation rates became less sensitive to temperatures. Near the melting points the rate is independent of temperature above an oxygen pressure of 10^{-5} atm. The bend in the Arrhenius plotted oxidation rate isobars occurs in the same temperature range as for tungsten. However, because of the lower melting point of molybdenum, an extended temperature independent region was not observed. Also, the molybdenum oxidation rates are slightly lower at high pressures and considerably higher at low pressures than the corresponding tungsten oxidation rates. It appears from the rate isobar at 1×10^{-6} atm that the reaction probability on molybdenum is not invariant with temperature. As a result of the variable reaction probability the boundary film treatment used for the tungsten oxidation case was not attempted.

Gulbransen, Andrew, and Brassart[25] measured molybdenum oxidation rates to 1700°C in 0.1 atm of oxygen. Their samples were oxidized in a closed end tube which restricted oxygen input and oxide vapor purging. This complicates

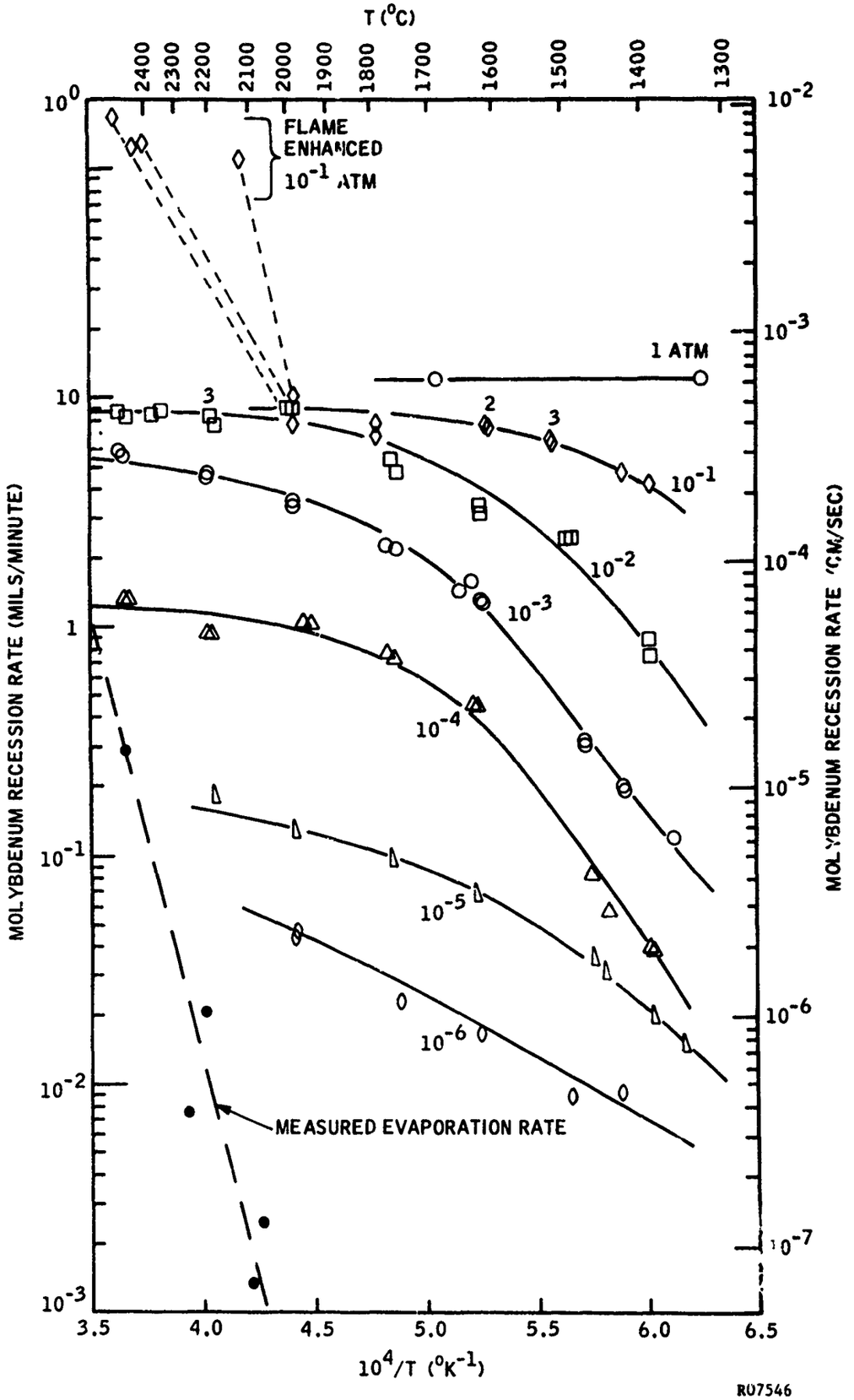

FIGURE 29. ARRHENIUS PLOT OF RECESSION RATES OF MOLYBDENUM

the boundary film analytical problem further but makes the rate more sensitive to gas flow. A comparison between their fastest rate data and the equivalent rate data from this study is shown in Figure 30. Both investigations are in reasonably good agreement. The molybdenum oxidation rates observed by Modisette and Schryer[24] in slow moving air above 1400°C vary between 1.3 and 2.8 mils/minute. This is about 1/5 the oxidation rate in pure oxygen of the same pressure, 0.21 atm. The lowered rate in air is in good agreement with the decrease expected because of nitrogen dilution based on equation (5). At the high partial pressures involved using air, the approximation $P_{O_2} \gg P_{O_{2(s)}}$ is valid and therefore:

$$\dot{X}_{Mo} = k_m \left(\frac{P_{O_{2\,\infty}}}{P_t} \right) \qquad (27)$$

the transport coefficient will not vary much in diluting oxygen with nitrogen because of the similar molecular weights of these gases, see equation (10). Since $P_{t(air)} = 5\ P_{O_{2\infty}}$ a rate reduction of 1/5 is expected, which conforms with the experimental results.

2. FLAME ENHANCED OXIDATION RATES

The most interesting aspect of oxidizing molybdenum at high temperatures and pressures was a large discontinuous increase in rates observed at high pressures. This change in rate is accompanied by a sudden rise in temperature, even though external heating is removed. Furthermore, the sample is surrounded by a typical gas flame, indicating the combustion of fuel in the gas phase rather than on the surface of the metal rod. Although oxidation of tungsten at 10^{-1} atm and 1 atm was self-supporting at high temperatures once initiated, the flame phenomena and recession rate increases were not observed with tungsten. The transition in behaviour associated with flame ignition is easily distinguished. Rods burning normally without an accompanying flame appear as bright incandescent objects. The surrounding cloud caused by condensation of molybdenum oxide particles can only be detected by reflected light. After flame ignition the reverse in light intensity occurs. The incandescent rod cannot be distinguished visually from the brilliant flame surrounding it, without filters. Prior to ignition, temperature cannot be detected by optical pyrometry within the vapor cloud. After igintion, the color temperature of the flame varies from 2200 to 2500°C in 0.1 atm of oxygen and between 2700°C and 2800°C in 1 atm of oxygen. These temperatures were recorded using the coloratio pyrometer and fields of view which excluded the sample rod. The high flame temperature associated with an oxygen pressure of 1 atm causes the sample to melt within a few seconds after flame ignition.

Rod diameters and recession rates can be measured photographically using filters. A typical rate curve is shown in Figure 31. Oxidation of the rod continues to obey a linear rate law after ignition but proceeds at a much faster rate. The flame enhanced oxidation rates were not plotted in Figure 29, but are listed in Table 5. At both 0.1 atm and 1 atm oxygen pressures, ignition

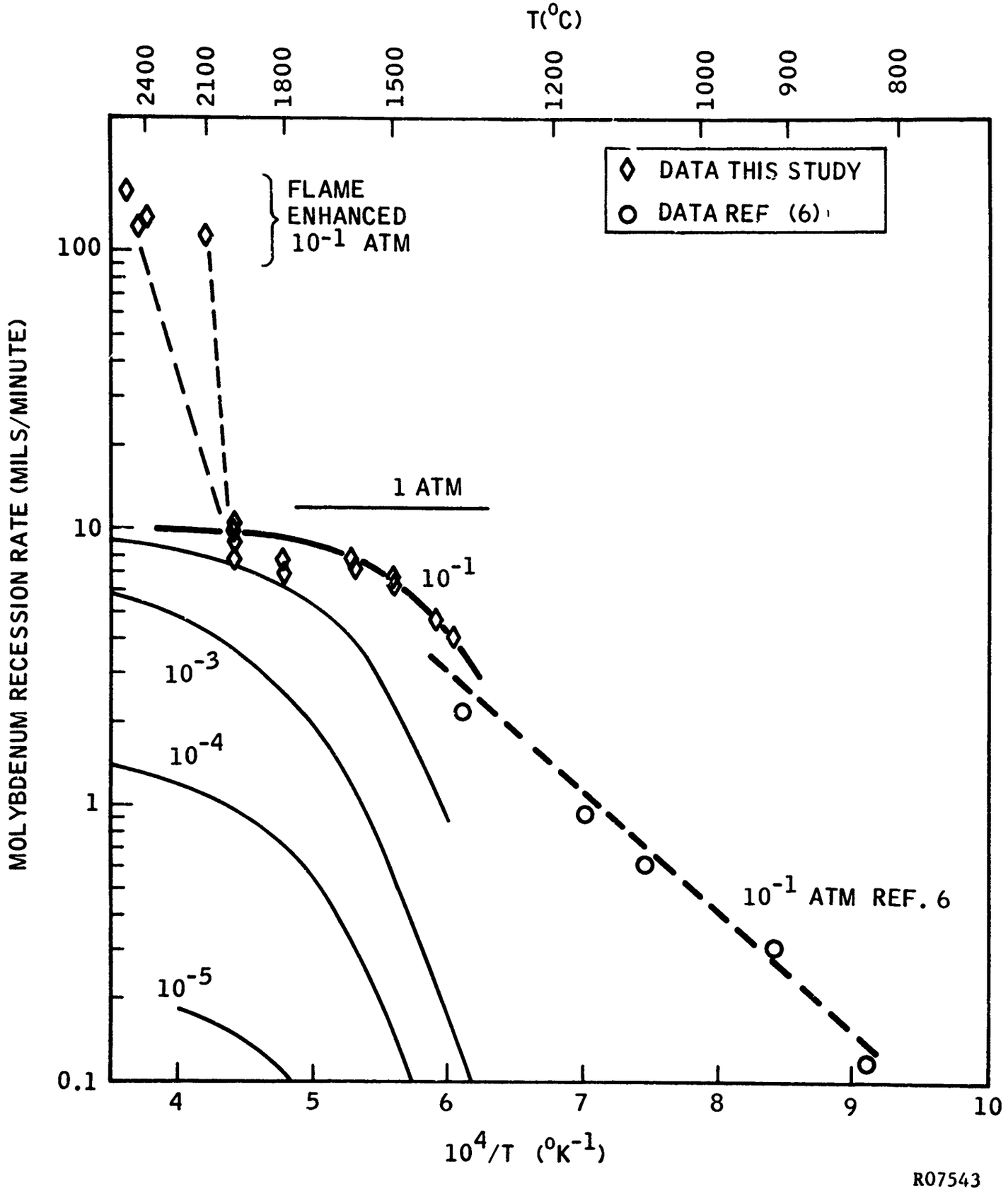

FIGURE 30. COMPARISON OF MOLYBDENUM OXIDATION RATES IN PURE OXYGEN AT 10^{-1} ATM: THIS STUDY AND GULBRANSEN, ANDREW, AND BRASSART[25]

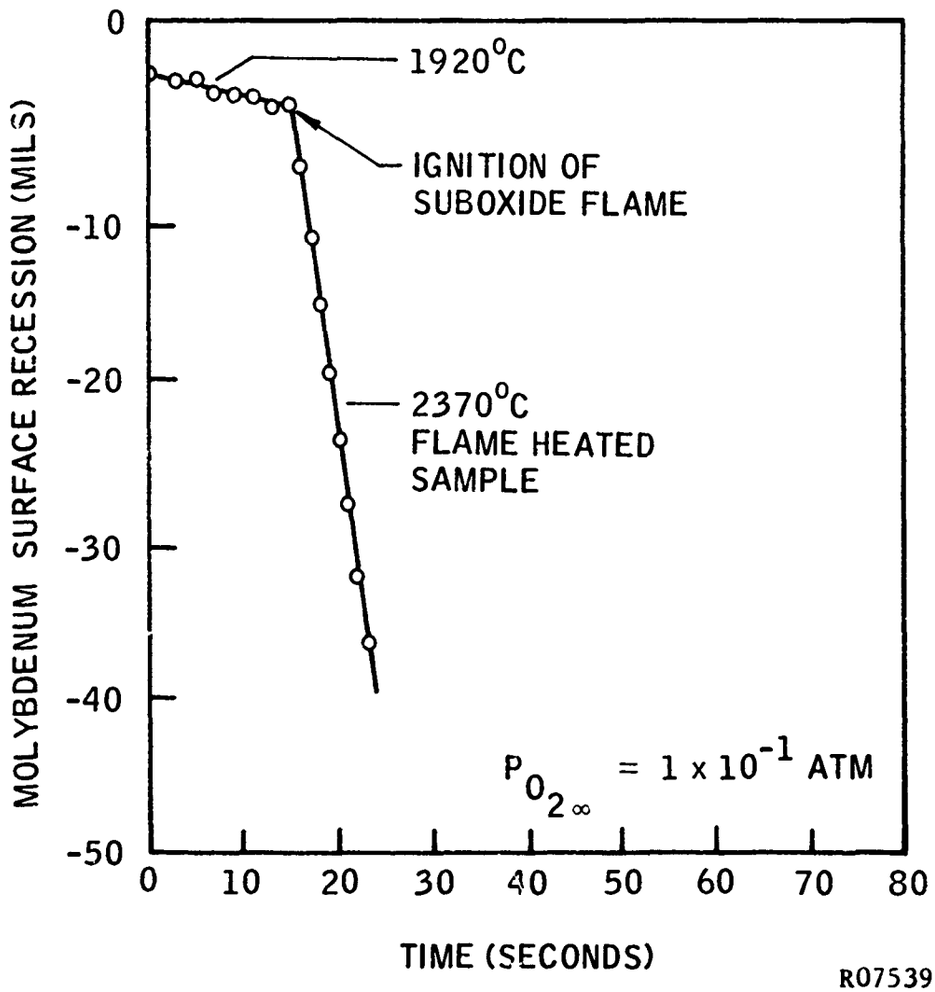

FIGURE 31. TRANSITION IN THE OXIDATION RATE OF MOLYBDENUM CAUSED BY IGNITION OF THE SUBOXIDE DIFFUSION FLAME AT 15 SECONDS

of the flame did not occur until a temperature of 1900°C was reached. This corresponds with the temperature at which $MoO_2(g)$ becomes appreciably more prevalent than $MoO_3(g)$ as the oxidation product determined by mass spectrometry[30]. This relation indicates that the flame results from the outward diffusion of the $MoO_2(g)$ and subsequent reaction with oxygen to product $MoO_3(g)$. Polymerization reactions are also strongly exothermic in this system. The heat released by these chemical reactions can produce the gaseous diffusion flame observed. Neglecting the small amount of $MoO_3(g)$ produced at the metal surface, the primary surface oxidation reaction is:

$$Mo + O_2 \longrightarrow MoO_2(g) \qquad (28)$$

The net secondary reaction in the gas phase, including polymerization to the dominant equilibrium species $(MoO_3)_3(g)$, is:

$$3/2\ O_2 + 3MoO_2(g) \rightleftharpoons (MoO_3)_3(g) \qquad \Delta H^o = -598 \text{ Kcal/Mole of product} \qquad (29)$$

This reaction is 50% more exothermic than the equivalent reaction in the tungsten system[2,3]:

$$3/2\ O_2 + 3WO_2(g) \rightleftharpoons (WO_3)_3(g) \qquad \Delta H^o = 405 \text{ Kcal/Mole} \qquad (30)$$

This difference in released heat provides a possible explanation for the presence of the diffusion flame with molybdenum under conditions where it is not observed with tungsten.

TABLE 5

EFFECT OF THE SUBOXIDE DIFFUSION FLAME ON MOLYBDENUM RECESSION RATES AT HIGH TEMPERATURES (TEMPERATURE INDEPENDENT REGION) AND HIGH OXYGEN PRESSURES

	P_{O_2} = 0.1 atm	P_{O_2} = 1 atm
Avg. Rate Without Flame	9 mils/minute	12 mils/minute
Avg. Rate With Flame	133 ± 25 mil/minute	470 mils/minute

REFERENCES

1. E. A. Kellet and S. E. Rogers, J. Electrochem. Soc. 110, 502 (1963).

2. P. E. Blackburn, M. Hoch, and H. L. Johnston, J. Phys. Chem. 62, 769 (1958).

3. J. Berkowitz, W. A. Chupka, and M. G. Inghram, J. Chem. Phys. 27, 85 (1957).

4. R. P. Burns, G. DeMaria, J. Drowart, and R. T. Grimley, J. Chem. Phys. 32, 1363 (1960).

5. J. Berkowitz, M. G. Inghram, and W. A. Chupka, J. Chem. Phys. 26, 842 (1957).

6. J. S. Dunn, J. Chem. Soc. 132, 1149 (1929).

7. E. A. Gulbransen and K. F. Andrew, J. Electrochem. Soc. 107, 619 (1960).

8. W. W. Webb, J. T. Norton, and C. Wagner, J. Electrochem. Soc. 103, 107 (1956).

9. R. Speiser and G. R. St Pierre, "Research on the Oxidation Behaviour of Tungsten," Ohio State Univ. Research Foundation, Columbus, Ohio; WADD Rept. 831-9, Contract AF 33(616)-5721, Oct. 1960.

10. J. P. Baur, D. W. Bridges, and W. M. Fassell, Jr., J. Electrochem. Soc. 103, 266 (1956).

11. E. A. Gulbransen, K. F. Andrew, and F. A. Brassart, J. Electrochem. Soc. 111, 103 (1964).

12. J. N. Ong, Jr., J. Electrochem. Soc. 109, 284 (1962).

13. I. Langmuir, J. Am. Chem. Soc. 105, 35 (1913); ibid 37, 1139 (1915).

14. J. Eisinger, J. Chem. Phys. 30, 412 (1959).

15. J. A. Becker, E. J. Becker, and R. G. Brandes, J. Appl. Phys. 32, 441 (1961).

16. H U. Anderson, "Kinetic Studies of the Reactions Occurring Between Tungsten and Gases at Low Pressures and High Temperatures," (Ph.D. Thesis, Univ. Calif. 1962); UCRL 10135, April 1962.

17. R. C. Peterson and W. M. Fassell, Jr., "High Pressure Oxidation of Metals--Molybdenum in Oxygen," Tech. Rept. No. 6, Sept. 1954. Army Ordnance Contract DA 04-495-ORD-237. Univ. of Utah.

18. M. Simnad and A. Spilners, J. Metals 7, 1011 (1955).

19. E. S. Bartlett and D. N. Williams, Trans. AIME 212, 280 (1958).

20. B. Lustman, Metals Progr. 57, 5 (1950).

21. E. A. Gulbransen and W. S. Wysong, AIME Metals Technol. 14, No. 6, Tech. Publ. No. 2226 (1947).

22. North American Aviation, Inc., "High Temperature Oxidation of Molybdenum Under High Altitude Conditions," Air Force Contract 33(600)-28469, ASTIA No. 147839, NAA Rept. No. AL-2617, Sept. 1957.

23. E. S. Jones, J. F. Mosher, R. Speiser, and J. Spretnak, Corrosion 14, 2t (1958).

24. J. L. Modisette and D. R. Schryer, "An Investigation of the Role of Gaseous Diffusion in the Oxidation of a Metal Forming a Volatile Oxide," NASA Tech. Note D-222, March 1960.

25. E. A. Gulbransen, K. F. Andrew, and F. A. Brassart, J. Electrochem. Soc. 110, 952 (1963).

26. J. A. Becker and C. D. Hartman, J. Phys. Chem. 57, 157 (1953).

27. C. R. Wilks, "Effects of Temperature, Pressure and Mass Flow on Oxidation of Molybdenum," SAMPE Eastern Division Meeting, MIT, Cambridge, Mass., May 1960.

28. R. A. Perkins and D. D. Crooks, J. of Metals 13, 490 (1961).

29. R. A. Perkins, W. L. Price, and D. D. Crooks, "Oxidation of Tungsten at Ultra-High Temperatures," Lockheed Report 6-90-62-98, November 1962, Sunnyvale, California.

30. Joan B. Berkowitz-Mattuck, A. Büchler, J. L. Engelke, and S. N. Goldstein, J. Chem. Phys. 39, 2722 (1963).

31. M. Jakob, Heat Transfer, Vol. I, John Wiley and Sons, New York, p. 525, 1949.

32. R. B. Bird, W. E. Stewart, and E. L. Lightfoot, Transport Phenomena, John Wiley and Sons, New York, 1960, chs. 1 and 16.

REFERENCES (Continued)

33. P. E. Blackburn, K. F. Andrew, E. A. Gulbransen, and F. A. Brassart, "Oxidation of Tungsten and Tungsten Based Alloys," WADC Tech. Report 59-575 Part II; Westinghouse Electric Corp., June 1961, p. 6.

34. W. D. Kingery, Introduction to Ceramics, John Wiley and Sons, New York (1960) ch. 10.

35. J. A. Becker in Solid State Physics, Vol. 7, edited by F. Seitz and D. Turnbull, Academic Press, New York (1958) p. 379-424.

36. A. H. Shapiro, The Dynamics and Thermodynamics of Compressible Fluid Flow, Vol. I, The Ronald Press Co., New York (1954) pp. 236-37.

37. T. F. Chilton and A. P. Colburn, Ind. Eng. Chem. 26, 1183 (1934).

38. T. K. Sherwood and R. L. Pigford, Absorption and Extraction, McGraw-Hill, New York (1952), 2nd ed., p. 70.

39. O. V. Mitrofanov, "Soviet Physics-Crystallography," 8, No. 2, 229-231 (Trans) (1963).

40. A. T. Gwathmey and K. R. Lawless, "The Influence of Crystal Orientation on the Oxidation of Metals," in The Surface Chemistry of Metals and Semiconductors, ed. by H. C. Gatos, John Wiley and Sons, New York, 1960, pp. 483-521.

41. H. W. Schadler, "Correlation of Etch Pits and Dislocations in Tungsten," in Direct Observations of Imperfections in Crystals, ed. by J. B. Newkirk and J. H. Wernick, Interscience Publishers, New York, 1962, pp. 593-608.

42. I. Berlec, J. Appl. Phys. 33, No. 1, 197 (1962).

43. B. W. Batterman, J. Appl. Phys. 28, 1236 (1957).

44. F. M. Wanlass and H. Eyring, "Sticking Coefficients," in Advances in Chemistry Series No. 33, p. 140, American Chemical Society, 1961.

45. J. P. Hirth and G. M. Pound, Condensation and Evaporation Progress in Materials Science, Vol. XI, The MacMillan Co., New York (1963), Chapter D.